Design, synthesis and biological evaluation of benzoylacrylic acid shikonin ester derivatives as irreversible dual inhibitors of tubulin and EGFR

Wen-Xue Sun, Hong-Wei Han, Min-Kai Yang, Zhong-Ling Wen, Yin-Song Wang, Jiang-Yan Fu, Yun-Ting Lu, Ming-Yue Wang, Jia-Xin Bao, Gui-Hua Lu, Jin-Liang Qi, Xiao-Ming Wang, Hong-Yan Lin, Yong-Hua Yang

PII: S0968-0896(19)31152-6
DOI: https://doi.org/10.1016/j.bmc.2019.115153
Reference: BMC 115153

To appear in: *Bioorganic & Medicinal Chemistry*

Received Date: 9 July 2019
Revised Date: 27 September 2019
Accepted Date: 3 October 2019

Please cite this article as: Sun, W-X., Han, H-W., Yang, M-K., Wen, Z-L., Wang, Y-S., Fu, J-Y., Lu, Y-T., Wang, M-Y., Bao, J-X., Lu, G-H., Qi, J-L., Wang, X-M., Lin, H-Y., Yang, Y-H., Design, synthesis and biological evaluation of benzoylacrylic acid shikonin ester derivatives as irreversible dual inhibitors of tubulin and EGFR, *Bioorganic & Medicinal Chemistry* (2019), doi: https://doi.org/10.1016/j.bmc.2019.115153

Design, synthesis and biological evaluation of benzoylacrylic acid shikonin ester derivatives as irreversible dual inhibitors of tubulin and EGFR

Wen-Xue Sun[1,2†], Hong-Wei Han[1,2†], Min-Kai Yang[1,2], Zhong-Ling Wen[1,2], Yin-Song Wang[1,2], Jiang-Yan Fu[1,2], Yun-Ting Lu[1,2], Ming-Yue Wang[1,2], Jia-Xin Bao[1,2], Gui-Hua Lu[1,2], Jin-Liang Qi[1,2]*, Xiao-Ming Wang[1,2]*, Hong-Yan Lin[1,2]*, Yong-Hua Yang[1,2]*

[1]*State Key Laboratory of Pharmaceutical Biotechnology, Institute of Plant Molecular Biology, School of Life Sciences, Nanjing University, Nanjing 210023, PR China*

[2]*Co-Innovation Center for Sustainable Forestry in Southern China, Nanjing Forestry University, Nanjing, 210037, PR China*

[†]These authors contributed equally to this work

*Corresponding author:

Yong-Hua Yang,

State Key Laboratory of Pharmaceutical Biotechnology,

Nanjing University,

Nanjing 210023, PR China.

Tel/Fax: 86-25-89686305,

Email: yangyh@nju.edu.cn.

Abstract: In this study, a series of shikonin derivatives combined with benzoylacrylic had been designed and synthesized, which showed an inhibitory effect on both tubulin and the epidermal growth factor receptor (EGFR). *In vitro* EGFR and cell growth inhibition assay demonstrated that compound PMMB-317 exhibited the most potent anti-EGFR (IC_{50} = 22.7 nM) and anti-proliferation activity (IC_{50} = 4.37 μM) against A549 cell line, which was comparable to that of Afatinib (EGFR, IC_{50} = 15.4 nM; A549, IC_{50} = 6.32 μM). Our results on mechanism research suggested that, PMMB-317 could induce the apoptosis of A549 cells in a dose- and time-dependent manner, along with decrease in mitochondrial membrane potential (MMP), production of ROS and alterations in apoptosis-related protein levels. Also, PMMB-317 could arrest cell cycle at G2/M phase to induce cell apoptosis, and inhibit the EGFR activity through blocking the signal transduction downstream of the mitogen-activated protein MAPK pathway and the anti-apoptotic kinase AKT pathway; typically, such results were comparable to those of afatinib. In addition, PMMB-317 could suppress A549 cell migration through the Wnt/*β*-catenin signaling pathway in a dose-dependent manner. Additionally, molecular docking simulation revealed that, PMMB-317 could simultaneously combine with EGFR protein (5HG8) and tubulin (1SA0) through various forces. Moreover, 3D-QSAR study was also carried out, which could optimize our compound through the structure-activity relationship analysis. Furthermore, the *in vitro* and *in vivo* results had collectively confirmed that PMMB-317 might serve as a promising lead compound to further develop the potential therapeutic anticancer agents.

Chemical compounds studies in this article：

Shikonin (PubChem CID: 479503); Maleic anhydride (PubChem CID: 7923); Colchicine (PubChem CID: 6167); Paclitaxel (PubChem CID: 36314); Afatinib (PubChem CID: 10184653); Benzene (PubChem CID: 241); Methylbenzene (PubChem CID: 1140); Fluorobenzene (PubChem CID: 10008); Chlorobenzene (PubChem CID: 7964); Bromobenzene (PubChem CID: 7961).

Keywords: Shikonin, benzoylacrylic, tubulin, epidermal growth factor receptor, anticancer

1. Introduction

With the continuous exploration of tumor biology and the application of targeted drug delivery methods, targeted drug therapy has gradually become a research hotspot as a result of its outstanding clinical advantages, which can target specific binding sites in the course of tumor treatment, improve the therapeutic effect and reduce the drugs-related side effects[1].

As a kind of receptor tyrosine kinase, epidermal growth factor receptor (EGFR) can induce a complicated signaling cascade reaction, which plays a vital part in the biological functions to regulate cell support, survival, adhesion, and migration[2]. Specifically, the EGFR protein signaling pathways include the mitogen-activated protein kinase (MAPK) pathway[3], the anti-apoptotic kinase AKT pathway[4, 5], and several DNA transcription-related pathways in nucleus apoptosis. Each signaling pathway is linked with each other, which is involved in the normal physiological activities of cells and the cancerization process[6]. Over-expression of EGFR may account for an important cause of tumor formation and proliferation, and specifically inhibiting the EGFR activity can restrain tumor growth[7].

There are a series of small molecular compounds being reported to inhibit the EGFR activity, which can compete with the transmembrane domain in EGFR receptor to block the self-phosphorylation of the receptor. The small molecular EGFR tyrosine kinase inhibitors can be mainly classified as three categories, including the reversible single-target EGFR inhibitor, reversible double-target EGFR/HER2 inhibitor and non-reversible EGFR inhibitor[8]. Typically, gefitinib (**Fig. 1**A) is a reversible single-target EGFR inhibitor, which can highly integrate with the EGFR receptor (it can compete

with the ATP binding site in EGFR receptor[9]) to inhibit cell proliferation, and promote cell cycle arrest at the G0/G1 phase, thus ultimately inducing apoptosis. Icotinib (**Fig. 1**B), regarded as the "domestic Iressa"[10], is mainly indicated for the advanced non-small cell lung cancer (NSCLC), and it is found in clinical data to have higher safety than gefitinib[11]. Erlotinib and Afatinib (**Fig. 1**C and D) are the efficient reversible and irreversible EGFR inhibitors, respectively[12], which can block the cell cycle at G1 phase[13, 14]. Notably, the above EGFR inhibitors have shared a similar mechanism and post an inevitable drug resistance. Therefore, the existing approach to avoid drug resistance is to develop the effective multi-target inhibitors.

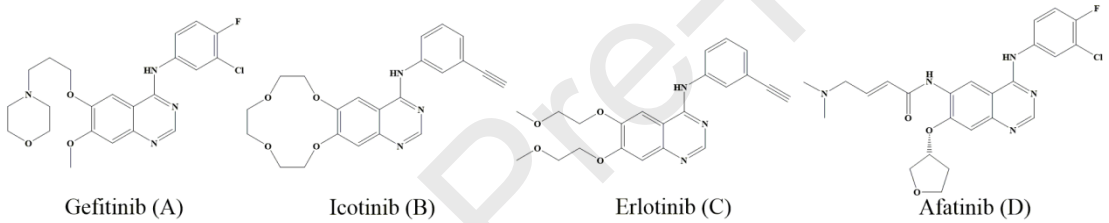

Fig. 1. Reported natural and synthetic EGFR inhibitors.

Notably, the *β*-Aroylacrylic acid derivatives have attracted wide attention because of their antibacterial, antitumor, fungicidal and other physiological activities; besides, they are also the important synthetic intermediates in the fields of medical science, agriculture, biology, and perfume[15]. The 4-phenyl-4-oxo-2-butenoic acid (benzoylacrylic acid) is structurally similar to chalcone and aroylacrylic acids, which has attracted our interest for further investigation since it can selectively and covalently combine the diverse pharmacological targets. In addition, results of 2D QSAR study had revealed the potency of such compounds in the covalent inhibition of EGFR.

Moreover, shikonin and its derivatives have possessed the antibacterial, anti-tumor,

antiviral, anti-inflammatory, anti-allergic and other pharmacological effects[16-18]. Our recent studies have mainly focused on obtaining the shikonin derivatives with high efficiency and low toxicity, and it is found that various types of modified shikonin derivatives have outstanding anti-tubulin activity[19]. Inspired by these previous research results, this study was mainly carried out aiming to design a kind of shikonin derivative with improved tumor targeting capacity. Typically, we would like to introduce a group of benzoylacrylic acid pharmacophore with EGFR-targeting inhibitory activity to the shikonin structure, which had combined a new type of reactive molecule containing both shikonin and benzoylacrylic acid. Results of activity validation had proved the function of this new molecular structure consisting of double enzyme or protein targets, together with various protein change-related regulatory pathways in the cell system. In addition, molecular docking simulation, along with other molecular activity detection, had rendered more reasonable molecular drug design.

2. Results

2.1 Chemistry

All the synthesized compounds for the benzoyl acrylic acid shikonin ester derivatives PMMB311-325 followed the general pathway outlined in **Scheme 1**. These compounds were obtained by two steps, which are elucidated in experimental section. All of them were firstly reported (**Table 1**) and characterized by ^{1}H NMR, ^{13}C NMR, melting test and mass spectroscopy in full accordance with depicted structures (***SI Appendix***). All docking runs were carried out by using CDOCKER Dock protocol of Discovery Studio 3.5.

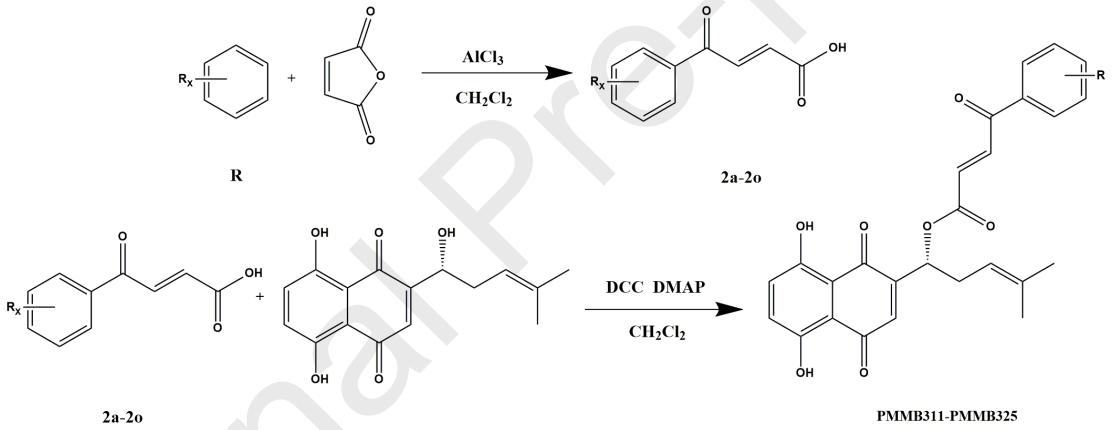

Scheme 1. Synthesis of compounds PMM-311~PMM-325. Reagents and conditions: (a) $AlCl_3$, CH_2Cl_2, reflux, 12 h; (b) DCC, DMAP, CH_2Cl_2, 0 °C, 4 h.

Table 1

Chemical structures and binding energy of PMM-311~PMM-325, Shikonin and Afatinib with 1SA0 and 5HG8.

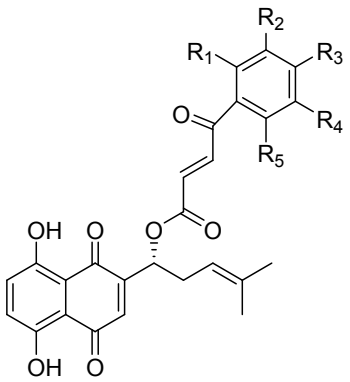

Compound	R_1	R_2	R_3	R_4	R_5	1SA0 ΔGb(kcal/mol)	5HG8 ΔGb(kcal/mol)	CC_{50} (μM) L02
PMMB-311	CH_3	H	H	CH_3	H	-60.25	-42.57	78.1
PMMB-312	H	H	CH_3	H	H	-52.13	-53.46	64.2
PMMB-313	H	CH_3	CH_3	H	H	-56.89	-49.34	88.4
PMMB-314	Cl	H	CH_3	H	H	-58.96	-52.11	> 100
PMMB-315	H	H	CH_2CH_3	H	H	-59.28	-56.36	92.4
PMMB-316	H	H	Cl	H	H	-60.46	-48.21	> 100
PMMB-317	H	H	F	H	H	-62.52	-58.76	89.2
PMMB-318	H	F	CH_3	H	H	-54.63	-45.86	> 100
PMMB-319	CH_3	H	CH_3	H	H	-56.73	-46.34	> 100
PMMB-320	H	Br	CH_3	H	H	-52.54	-48.54	> 100
PMMB-321	CH_3	H	H	Cl	H	-49.37	-49.03	83.3
PMMB-322	H	H	H	H	H	-53.66	-55.54	> 100
PMMB-323	F	H	CH_3	H	H	-60.42	-50.46	> 100
PMMB-324	CH_3	H	H	F	H	-64.35	-48.52	93.5
PMMB-325	H	H	Br	H	H	-54.69	-51.64	> 100
Shikonin						-65.53	-54.13	12.2
Afatinib						-54.85	-57.37	25.3

2.2 Bioactivity

2.2.1. PMMB-317 selectively inhibits cancer cells proliferation

MTT assay were performed for antiproliferative activities by the new compound PMMB311-325 against five human cancer cell lines, including the human breast cancer cells (MCF-7), human cervical cancer cells (HeLa), human non-small cell lung cancer cell lines (NCI H1975), human lung adenocarcinoma cell line (A549), human lung carcinoma cells (NCI H460) and human normal liver cell line (L02). Results showed in **Table 1** indicated that all compounds had lower cytotoxic against the non-tumorigenic L02 cells than shikonin itself. As shown in **Table 2**, almost all the compounds showed the anti-proliferative activities, Specifically, PMMB-317 (IC_{50} = 4.37 ± 0.46 μM) performed better anti-proliferation activities than afatinib (IC_{50} = 6.32 ± 1.57 μM) and shikonin (IC_{50} = 6.13 ± 1.68 μM) against A549 cells. Based on these results, we speculated that intervention of benzoyl acrylic acid derivatives could increase the anti-proliferative activities against cancer cells but significantly reduce the cytotoxicity of shikonin against non-cancer cells. To further investigate the anti-cancer mechanisms of these drugs, we chose compound PMMB-317 against A549 cells for downstream application.

Table 2

In vitro cell proliferation of compounds PMMB-311~ PMMB-325, Shikonin and Afatinib against five cancer cell lines.

Compound	IC_{50} ± SD (μM)				
	Hela	MCF-7	A549	H460	H1975
PMMB-311	10.15 ± 0.24	5.28 ± 0.17	13.13 ± 0.75	13.21 ± 1.67	10.19 ± 0.96
PMMB-312	8.96 ± 0.25	9.14 ± 0.41	9.72 ± 1.94	11.43 ± 2.44	10.17 ± 0.66
PMMB-313	10.13 ± 1.36	14.32 ± 1.82	9.12 ± 1.82	11.33 ± 1.42	15.68 ± 0.58

PMMB-314	10.13 ± 1.45	6.63 ± 0.53	6.23 ± 1.1	8.16 ± 1.21	9.56 ± 1.29
PMMB-315	15.23 ± 2.58	9.37 ± 1.33	14.54 ± 0.63	16.35 ± 1.41	12.39 ± 0.22
PMMB-316	11.42 ± 2.52	9.62 ± 0.69	8.52 ± 0.61	11.71 ± 1.23	11.85 ± 0.29
PMMB-317	7.93 ± 0.49	8.90 ± 0.13	4.37 ± 0.46	5.61 ± 1.03	9.43 ± 1.26
PMMB-318	8.27 ± 1.16	7.68 ± 1.23	9.39 ± 1.81	10.12 ± 2.53	7.25 ± 0.92
PMMB-319	18.55 ± 2.37	7.89 ± 1.2	10.18 ± 0.98	9.17 ± 1.23	16.55 ± 0.82
PMMB-320	17.15 ± 2.28	14.28 ± 0.49	15.37 ± 1.31	4.21 ± 0.45	22.54 ± 1.66
PMMB-321	9.34 ± 0.25	18.60 ± 0.44	13.22 ± 1.74	10.32 ± 0.71	18.28 ± 1.03
PMMB-322	17.56 ± 0.65	19.43 ± 2.18	7.51 ± 1.28	4.59 ± 0.03	10.26 ± 1.09
PMMB-323	15.1 ± 1.84	6.64 ± 0.36	12.63 ± 0.57	13.63 ± 2.5	9.56 ± 0.99
PMMB-324	14.21 ± 2.68	10.08 ± 1.45	13.42 ± 0.59	8.35 ± 1.32	7.26 ± 0.42
PMMB-325	8.02 ± 0.19	9.31 ± 0.43	9.19 ± 0.53	6.51 ± 0.98	13.28 ± 0.94
Shikonin	7.84 ± 0.67	9.55 ± 1.43	6.13 ± 1.68	5.04 ± 1.18	4.28 ± 1.08
Afatinib	6.39 ± 0.58	7.62 ± 2.35	6.32 ± 1.57	6.14 ± 0.67	5.55 ± 1.26

IC_{50}, the mean value of three separate determinations.

2.2.2. In vitro EGFR inhibitory activities

The EGFR inhibitory activities of all the synthesized shikonin derivatives were further evaluated in *vitro*. As shown in **Table 3**, all the tested compounds exhibited EGFR inhibitory activity at varying degree and some of them are even comparable to that of afatinib. Especially, compound PMMB317 (IC_{50} = 22.7 nM) and PMMB324 (IC_{50} = 23.4 nM) inhibited the EGFR activity remarkably, which was at least 6-fold stronger than shikonin (IC_{50} =139.2 nM) and almost comparable to afatinib (IC_{50} = 15.4 nM). Generally, the substituent groups on the aromatic ring affected the activity significantly. According to the structure-activity relationship, we clearly found that compounds with substitution on the phenyl ring enhanced inhibitory activities. Moreover, electron-withdrawing group (F, Cl) improved the enzymatic inhibitory

activity more significantly than the electron donating group (Et, Me).

Table 3

The EGFR inhibitory activity of PMMB-311~PMMB-325, Shikonin and Afatinib.

Compound	EGFR kinase	
	% inhibition at 150 nM	IC_{50} (nM)
PMMB-311	40.6	>150
PMMB-312	67.1	45.2
PMMB-313	55.8	118.6
PMMB-314	59.1	105.3
PMMB-315	65.3	50.8
PMMB-316	76.1	32.5
PMMB-317	80.3	22.7
PMMB-318	59.5	107.2
PMMB-319	40.9	>150
PMMB-320	33.1	>150
PMMB-321	50.1	146.2
PMMB-322	19.4	>150
PMMB-323	56.3	120.2
PMMB-324	83.3	23.4
PMMB-325	54.6	119.7
Shikonin	50.9	139.2
Afatinib	85.6	15.4

2.2.3. PMMB-317 caused cell apoptosis in a dose- and time- dependent manner

To evaluate the cell inhibitory activity of the compound PMMB-317, we conducted the cellular apoptosis assay. A549 cells were treated with PMMB-317 at various concentrations (0, 2, 4, 8 and 12 μM) for 24 h and 8 μM for 0, 12, 24 and 36 h at 37 ℃. As shown in **Fig. 2**A to D, with increasing concentrations or time of PMMB-317, the

percentage of apoptotic cells significantly increased, which suggested that PMMB-317 induced apoptosis in a time- and dose-dependent fashion. Additionally, we observed that PMMB-317 could significantly decrease Bcl-2, caspase-3 and caspase-9, but increased Bax protein expression and the cleavage of PARP, caspase-3 and caspase-9 in A549 cells, which was in full accordance with cell apoptosis results by western blotting. (**Fig. 2**E to H). Treatment with PMMB-317 at 4 μM and 8 μM for 24 h induced 28.20% and 66.10% cells apoptosis respectively. Notably, 18.92% and 59.2% cells induced apoptosis when treated with PMMB-317 at 8 μM for 12 h and 24 h respectively. Hence, it was concluded that PMMB-317 had a better ability to induce cell apoptosis especially at lower concentration and shorter time.

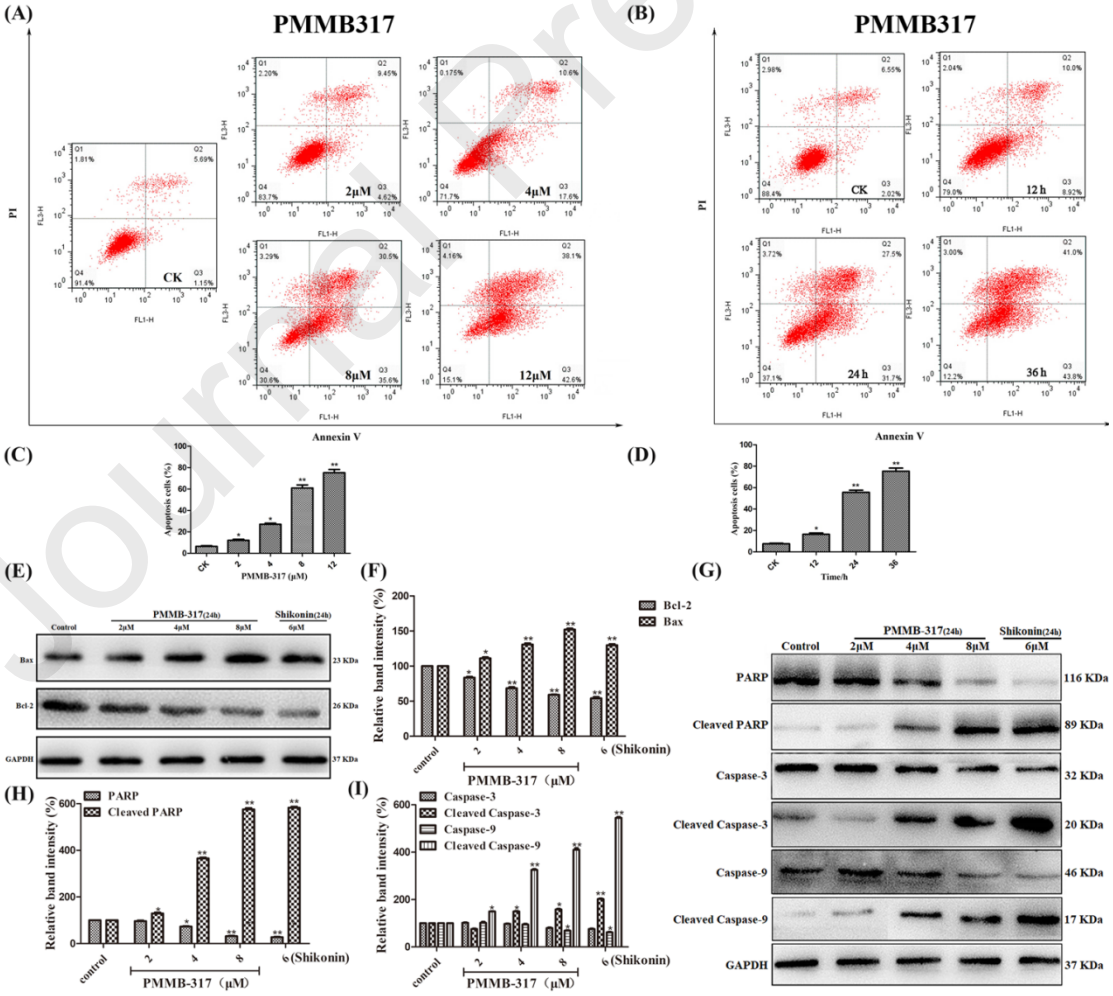

Fig. 2. PMMB-317 induced cell apoptosis in A549 cells. (A) PMMB-317 induced cell apoptosis in A549 cells in a dose-dependent manner. (B) PMMB-317 induced cell apoptosis in A549 cells in a time-dependent manner. (C) The percentage of apoptotic cells in A549 cells treated with various concentrations of PMMB-317 for 24 h. (D) The percentage of apoptotic cells in A549 cells treated with 8 μM PMMB-317 for different time. (E) Western blot analyses of apoptosis-related proteins (Bax, Bcl2) separated by SDS-PAGE. (F) Relative expression level was analyzed by Image J software. GAPDH served as a loading control. Images are representative of three independent experiments. Data are mean ± S.E.M. from three independent experiments (*P < 0.05; **P < 0.01). (G) Western blot analyses of apoptosis-related proteins (PARP, cleaved PARP, Caspase 3, cleaved caspase 3, Caspase 9 and cleaved caspase 9) separated by SDS-PAGE. (H) and (I) Relative band intensity was determined by Image J software. GAPDH served as a loading control. Images are representative of three independent experiments. Data are mean ± S.E.M. from three independent experiments (*P < 0.05; **P < 0.01).

2.2.4. PMMB-317 could induce the early apoptosis in a dose-dependent manner

The early apoptosis of cells is accompanied by production of ROS and the decrease of MMP[20]. After treatment with 4, 8 or 12 μM of PMMB-317, microscopy revealed that in untreated A549 cells, the pattern of well-polarized mitochondria marked by red fluorescent staining was replaced by green fluorescence (**Fig. 3**). In addition, flow cytometry showed that the percentage of cells with high membrane potential decreased from 90.6% to 67.8% after exposure to 4 μM PMMB-317 for 12 h and even decreased

to 38.6% in 12 μM PMMB-317 treated group. To eliminate the impact of late apoptosis on MMP depolarization, cells were treated with PMMB-317 for only 12 h, and through the PI staining results, there was scarely any late apoptotic cells.

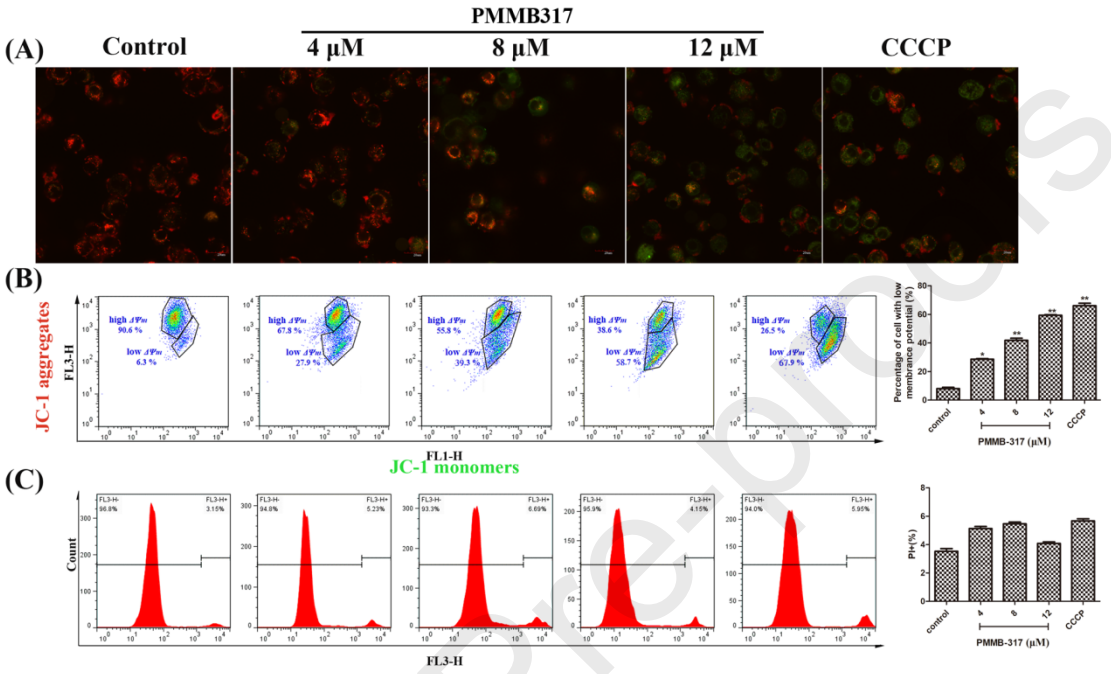

Fig. 3. Mitochondrial transmembrane potential was analysed in PMMB-317-treated A549 cells by JC-1 staining. (A) Cytofluorimetric analysis of mitochondrial membrane potential ($\Delta\Psi m$) by JC-1 staining. (B) Flow cytometry analysis of A549 cells with high $\Delta\Psi m$ (%) by JC-1 staining. (C) Flow cytometry analysis of A549 cells present PI positive. Each point represents the mean ± S.E.M. from three replicates (**P < 0.01).

Moreover, ROS generation represent a result of intracellular mitochondrial depolarization according the previous study[21]. Therefore, it is essential for us to investigate whether the PMMB-317 could induce ROS production in A549 cells. As shown in **Fig. S**1, ROS inducing ability were significantly increased with the treatment of PMMB-317 in a dose dependent manner. Taken together, all of these can further

confirm that PMMB-317 could induce the early apoptosis of A549 cells in a dose-dependent manner.

2.2.5. Effect of PMMB-317 on cell cycle arrest

Then to elucidate whether the anti-proliferative effect induced by the derivatives was due to cell cycle arrest, A549 cells were treated with the compound PMMB-317. According to the data illustrated in **Fig. 4**A to D, treatment of A549 cells with compound PMMB-317 lead to G2/M arrest in a dose and time mechanism. When the concentration of PMMB-317 increased to 8 μM, 33.01% of cells showed G2/M phase arrest compared with the control groups. Consistently, 46.55% of cells showed G2/M arrest, when the treatment time was 36 h. In keeping with the result, immunoblot analysis of cell cycle related proteins, Cyclin A, CDK1 and CDK2 were performed. As shown in **Fig. 4**E and F, the accumulation levels of CDK1 markedly increased compared to the control group, which indicated that the G2/M arrest was induced by PMMB-317. while the level of cyclin A and CDK1 were moderately down regulated. Therefore, we predict that PMMB-317 was not very efficient to induce cell apoptosis via cell cycle arrest.

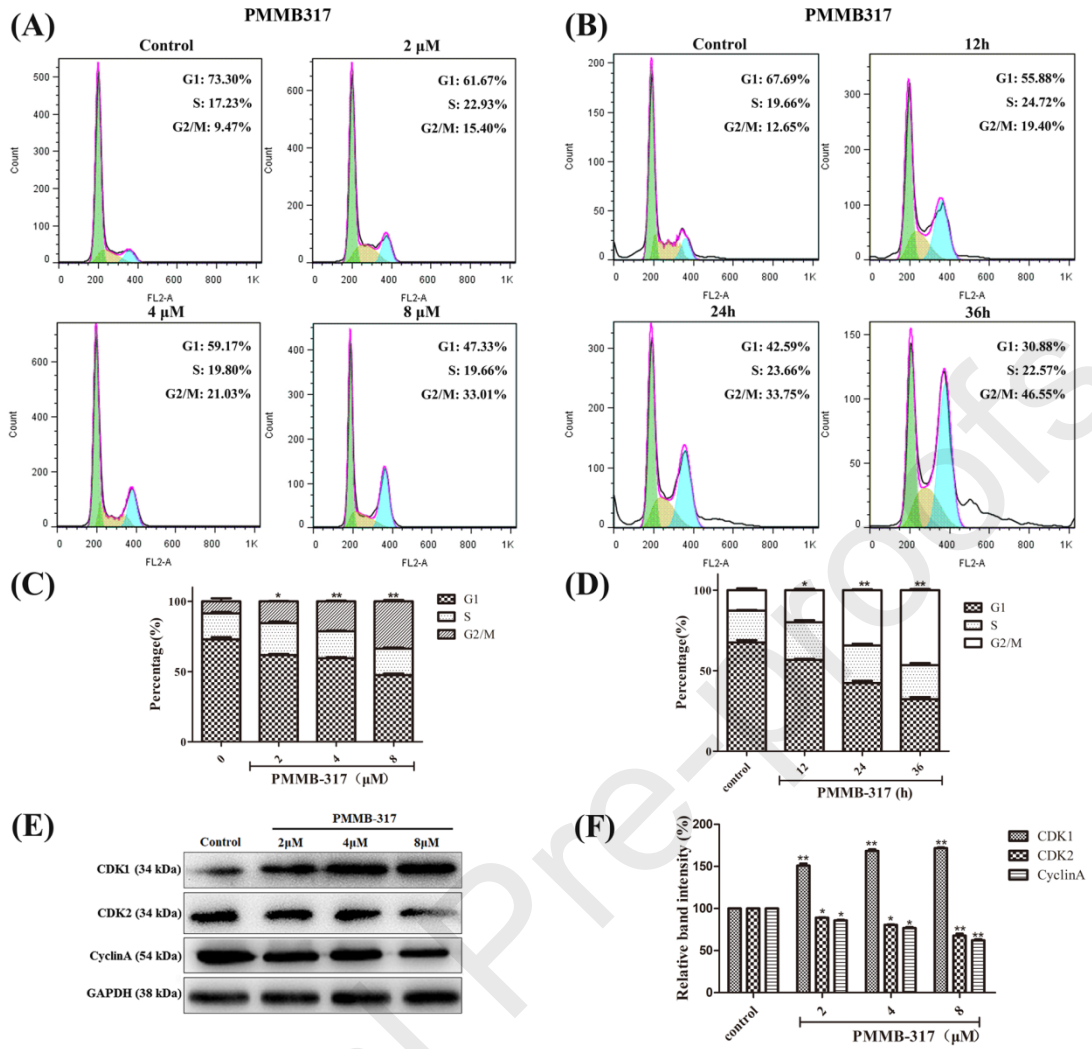

Fig. 4. The effects of different concentrations of PMMB-317 on cell cycle distribution in A549 cells. (A) Cells were treated with 0, 2, 4, 8 μM PMMB-317 for 24 h. (B) Cells were treated with 8 μM PMMB-317 for different time (G1 phase, green; S phase, yellow and G2/M phase, blue). (C) Statistic analysis of dose-dependent assay. (D) Statistic analysis of time-dependent assay. (E) Representative image of immunoblot analysis of cell cycle related proteins in A549 cells treated with PMMB-317. (F) Relative band intensity was determined by Image J software. GAPDH served as a loading control. Images are representative of three independent experiments. Data are mean ± S.E.M. from three independent experiments (*P < 0.05; **P < 0.01).

2.2.6. Effect of PMMB-317 on the cytoskeleton architecture of A549 cells

Confocal laser experiments can be used to observe the morphology of cell microtubules under the action of drugs, previous cell cycle experiment showed that the compound PMMB-317 could block the A549 cell cycle in G2/M phase, thus affecting cell growth and proliferation. In view of previous reports that the polymerization and depolymerization of microtubules could influence the cell cycle. To confirm that, the depolymerization or aggregation of microtubules were observed under confocal laser scanning microscope. As shown in **Fig. 5**, the compound PMMB-317 could lead to tubulin depolymerization distinctly just like colchicine treated group. The initial result prompt us to further investigate, microtubule assembly assay was conducted *in vitro*. PMMB-317 and colchicine caused inhibition of microtubule assembly at the concentration of 4, 8 μM and 1 μM for 24 h respectively, while paclitaxel promoted the polymerization of tubulin significantly at the concentration of 1 μM (**Fig. 5**B and C).

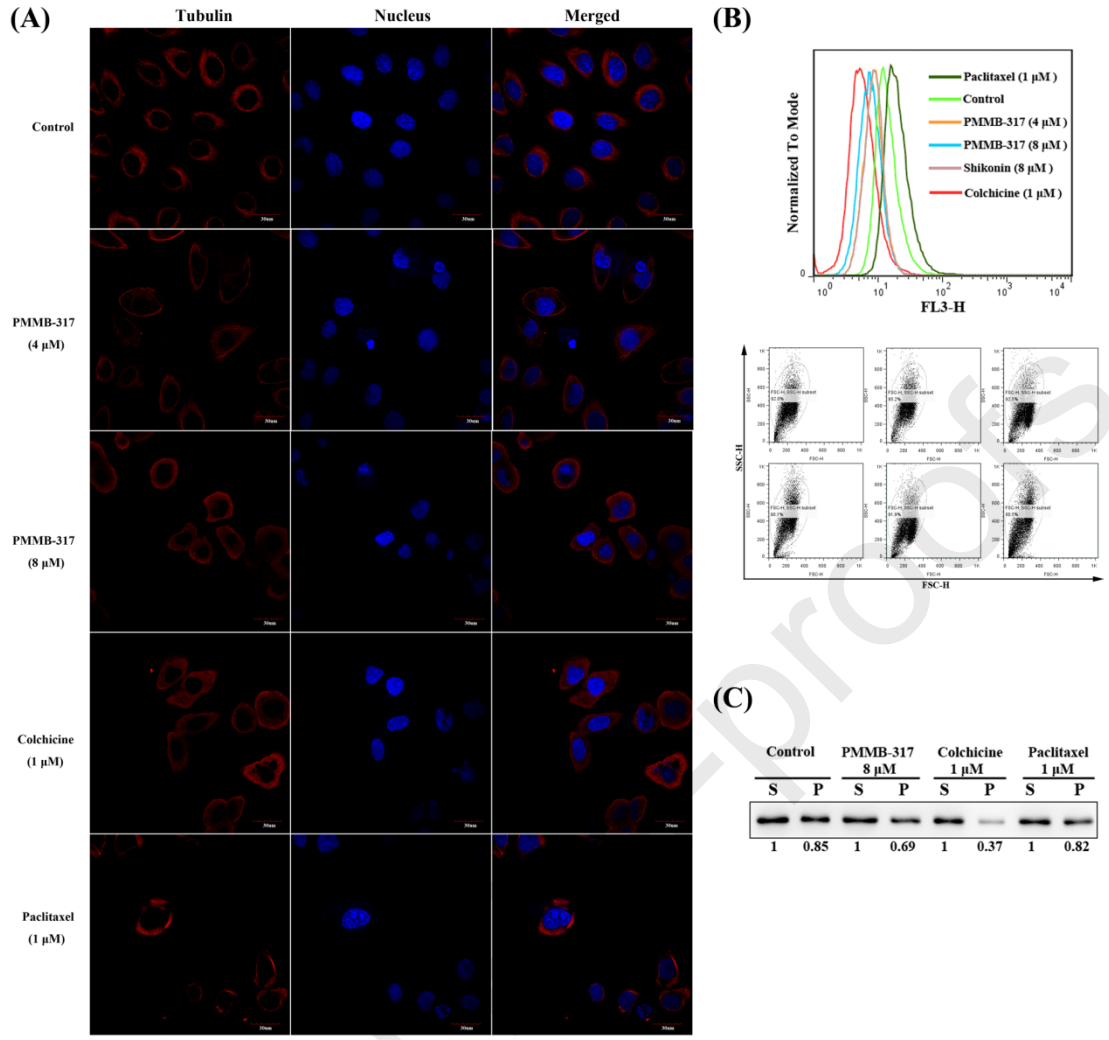

Fig. 5. Effect of PMMB-317 on the interphase microtubules of A549 cells using colchicine and paclitaxel as references. (A) Microtubules tagged with rhodamine (red) and nuclei tagged with DAPI (blue) were observed under a confocal microscope. (B) PMMB-317 affected microtubule assembly *in vitro*. After 24 h treatment with PMMB-317 (4, 8 μM), colchicine (1 μM), and paclitaxel (1 μM), polymerized tubulin on the cell membrane was immunoblotted with b-tubulin antibody and detected by flow cytometry. (C) PMMB-317 affected microtubule assembly in *vitro*. After treating A549 cells with PMMB-317 (4, 8 μM), colchicine (1 μM), and paclitaxel (1 μM) for 24 h, cytosolic (S, soluble) and cytoskeletal (P, polymerized tubulin) tubulin fractions were separated and immunoblotted with antibody against *β*-tubulin.

2.2.7. Effect of PMMB-317 on cell migration of A549 cells

Tumor cell migration undoubtedly increases the difficulty of curing tumors, especially once the distal metastasis occured[21]. To investigate whether PMMB-317 could inhibit the migratory capacity of A549 cells, the conventional in vitro wound healing assay was conducted. As shown in **Fig. 6**A and B, the control group cells gradually occupied the cell-free space within the channel over time and the cells almost filled the channel after 48 h. Whereas, cells migration capacity was greatly inhibited in a dose-dependent manner exposure to PMMB-317. The Wnt/*β*-catenin signaling pathway is vital for many cellular processes including cell proliferation and migration[21]. Based on the above results, we subsequently investigated the influence of PMMB-317 on Wnt/*β*-catenin signaling pathway in A549 cells. Western blot analysis results shown in **Fig. 6**C indicated that PMMB-317-treated A549 cells resulted in a decreased expression of *β*-catenin in cytoplasm and an increased protein expression of Axin-2 in a dose-dependent manner. These results together suggest that PMMB-317 might inhibit migration of A549 cells via Wnt/*β*-catenin signaling pathway.

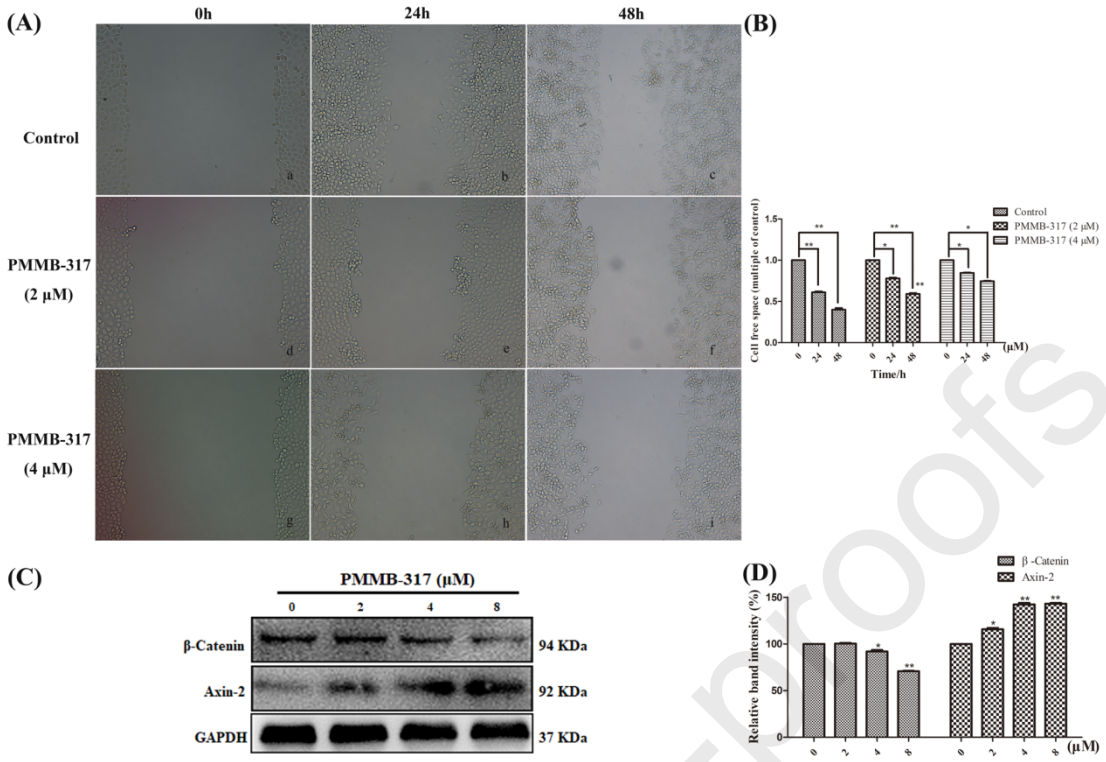

Fig. 6. The effects of PMMB-317 on cell migration in A549 cells. (A) Cell migration was detected by the wound scrape assay. Representative images of cell migration in the wound scrape model at 0, 24 and 48 h are shown. (B) Statistical analysis of the wound scrape assay. (C) Western blot analyses of Wnt/*β*-catenin signaling pathway proteins (*β*-catenin and Axin-2) separated by SDS-PAGE. (D) Relative band intensity was determined by Image J software. GAPDH served as a loading control. Images are representative of three independent experiments. Data are mean ± S.E.M. from three independent experiments (*P < 0.05; **P < 0.01).

2.2.8. Effect of PMMB-317 on EGFR signaling pathway of A549 cells

EGFR activation has been connected to multiple biological processes in cancer progression, such as cell migration, proliferation and metastasis through many signaling pathways[22]. To investigate the effect of PMMB-317 on EGFR, we conducted

immunoblot analysis of EGFR and its downstream signaling pathways proteins. As shown in **Fig. 7**, A549 cells that expressed high EGFR was treated with increasing concentrations of PMMB-317 and demonstrated a dose-dependent decrease in phosphorylation of EGFR, ERK and AKT.

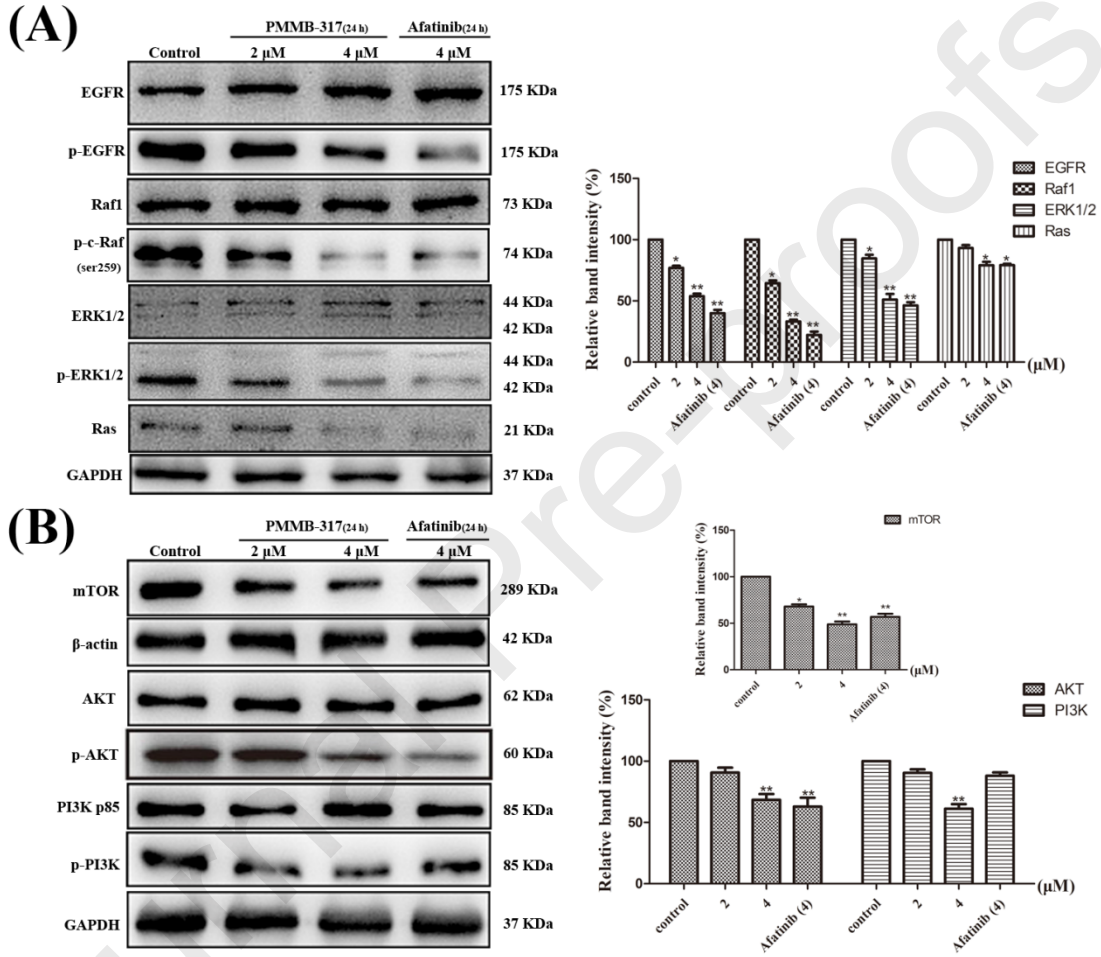

Fig. 7. The effects of PMMB-317 on EGFR signaling pathway in A549 cells. (A) Western blot analyses of apoptosis-related proteins (p-EGFR, Ras, p-c-Raf, ERK1/2, p-ERK1/2) separated by SDS-PAGE. Relative band intensity was determined by Image J software. GAPDH served as a loading control. Images are representative of three independent experiments. Data are mean ± S.E.M. from three independent experiments (*P < 0.05; **P < 0.01). (B) Western blot analyses of apoptosis-related proteins (p-

PI3K, AKT, p-AKT, mTOR) separated by SDS-PAGE. Relative band intensity was determined by Image J software. GAPDH and *β*-actin served as a loading control. Images are representative of three independent experiments. Data are mean ± S.E.M. from three independent experiments (*P < 0.05; **P < 0.01).

2.2.9. PMMB-317 effectively supress tumor growth of A549 xenografts in nude mice model

To evaluate the antitumor effects of PMMB-317 *in vivo*, we subcutaneously inoculated A549 cells into the left flank of female nude mice. Two weeks later, all the mice got visible tumors. The mice were then randomized into 5 groups. Changes in tumor volumes and body weight were measured and recorded after every two days. As shown in **Fig. 8**B and C, PMMB-317 inhibited the tumor growth compared with control in a dose-dependent manner. After the last treatment on day 32, average tumor size of PMMB-317 (4 mg/kg) was 6-fold smaller than vehicle control group (**Fig. S**2). The effect of PMMB-317 was similar to that of Afatinib at 4 mg/kg dose and better than Shikonin (2 mg/kg) treated group. However, PMMB-317 had no significant effect on body weight of mice while shikonin caused a significant decrease in body weight compared with the control group. Therefore, we speculated that the inhibitory effect of PMMB-317 on tumor growth was increased and its cytotoxicity was reduced significantly compared with shikonin. Meanwhile, overall survival of mice in PMMB-317-treated groups were greatly increased (**Fig. 8**E).

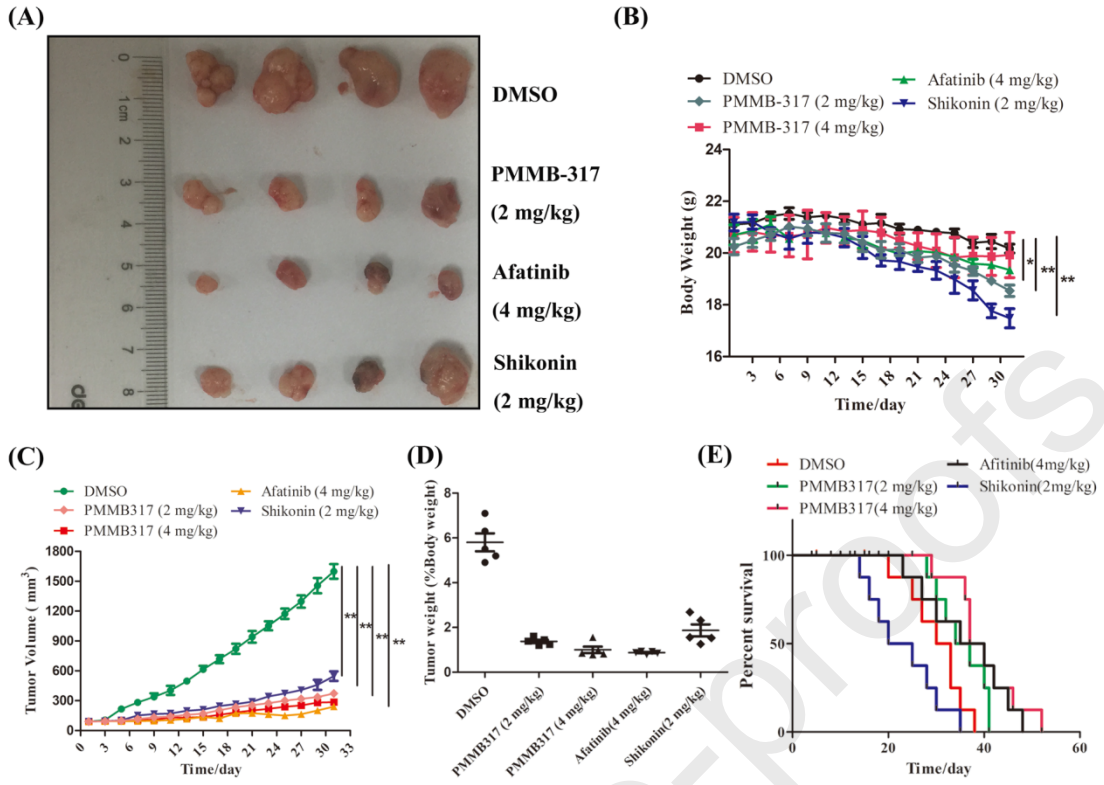

Fig. 8. PMMB-317 suppresses tumor growth of A549 xenografts in nude mice. (A) Four representative tumors were shown. (B) Body weight of the mice. (C) Tumor volumes of the mice. (D) The percentage of tumor weight were calculated. (E) Survival curve of mice. Data are the mean ± S.E.M. of 8 mice per group. (*P < 0.05; **P < 0.01 versus vehicle (DMSO)).

2.3. Molecular docking

Docking study has confirmed that PMMB-317 conjugated in the colchicine site of tubulin (PDB: 1SA0) perfectly. As shown in **Fig. 9**A and B, compound PMMB-317 binds to tubulin (PDB: 1SA0) with CDOCK interaction energy of -62.52 kcal/mol (**Table 1**) via three hydrogen bonds with ASN 101 and 258, LYS254. Other weak interactions, such as van der Waals and carbon-hydrogen bonds, also contribute to the binding affinity of compound PMMB-317 with tubulin. In addition, as shown in **Fig.**

9C and D, PMMB-317 also binds to EGFR (PDB: 5HG8) with CDOCK interaction energy of -58.76 kcal/mol (**Table 1**) via two hydrogen bonds with ARG 841 and CYS 797.

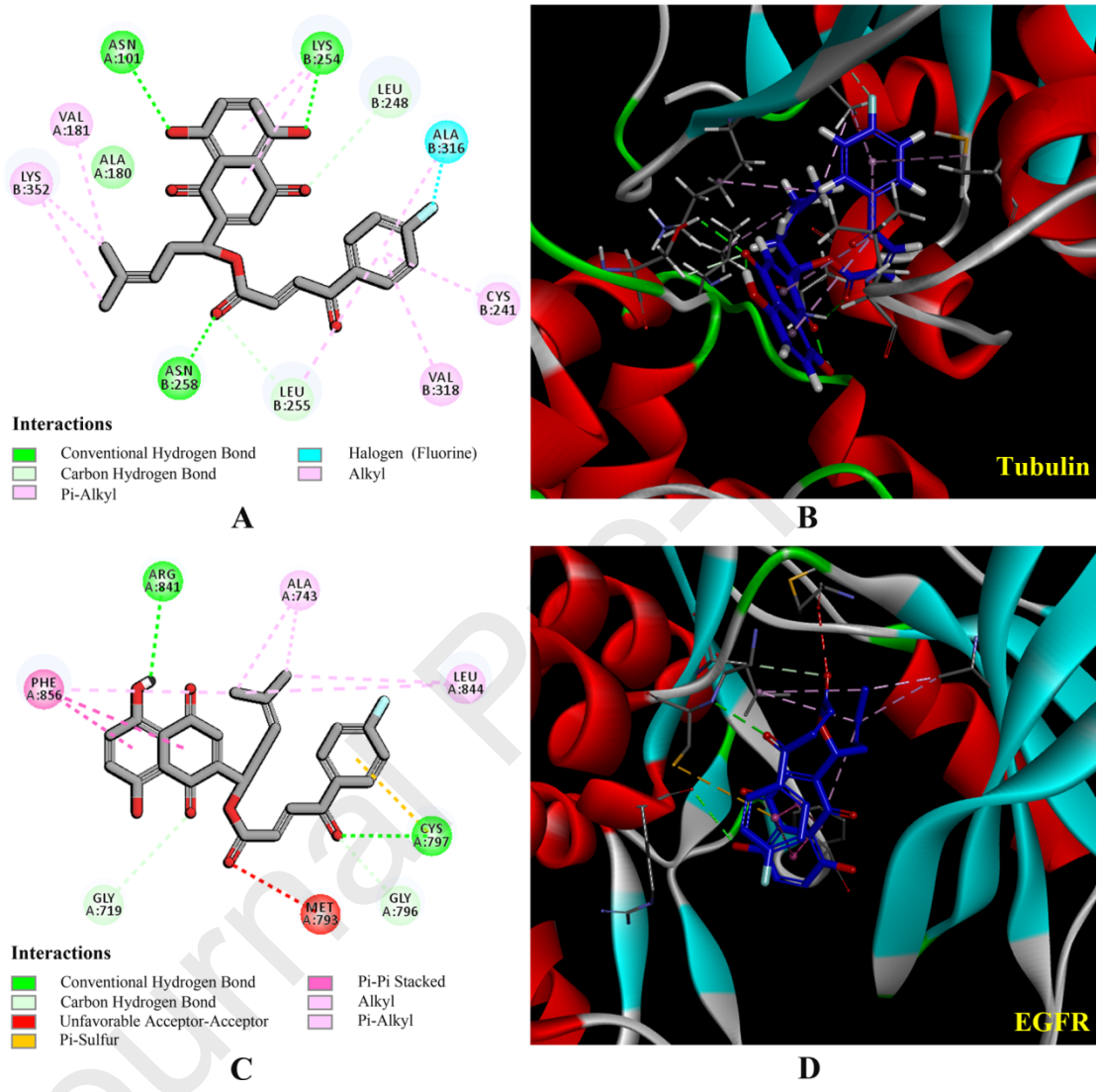

Fig. 9. Molecular docking model of compound PMMB-317 with the tubulin (PDB code 1SA0) and EGFR (PDB code 5HG8) binding sites. (A) Interactions of PMMB-317 with the amino acid residues at the binding pocket of tubulin (carbon atom, gray; oxygen atom, red; fluorine atom, light green). (B) Binding pose of PMMB-317 in the protein surface of tubulin (carbon atom, blue; oxygen atom, red; hydrogen atom, white; fluorine atom, bright green). Hydrogen bonds were displayed as green dashed lines. (C)

Interactions of PMMB-317 with the amino acid residues at the binding pocket of EGFR (carbon atom, gray; oxygen atom, red; fluorine atom, light green). (D) Binding pose of PMMB-317 in the protein surface of EGFR (carbon atom, blue; oxygen atom, red; hydrogen atom, white; fluorine atom, bright green). Hydrogen bond was displayed as green dashed lines.

2.4. 3D-QSAR analysis

In order to get a better interaction of small molecules with target protein, 3D-QSAR was used to optimize the small molecules and the calculations were done by built-in QSAR software of DS 3.5 (Discovery Studio 3.5, Accelrys, Co. Ltd). Eighteen compounds were utilized to 3D-QSAR study and pIC_{50} was transformed from the available IC_{50} (μM) values of anti-proliferation assay. Compounds PMMB259[23] and 8b[24], have been found in the previous research of our laboratory which had similar structure to benzoylacrylic acid shikonin ester derivatives that were involved in the 3D-QSAR study to satisfy the minimum requiments of the computer simulation. All compounds were divided into the training and test parts, which are shown in **Table S**1. The correlation co-efficient R^2 of this model was 0.9987, which manifests this model has an ability to predict. The distribution between predicted pIC_{50} and experimental pIC_{50} value for both test sets and training sets were shown in **Fig. 10**.

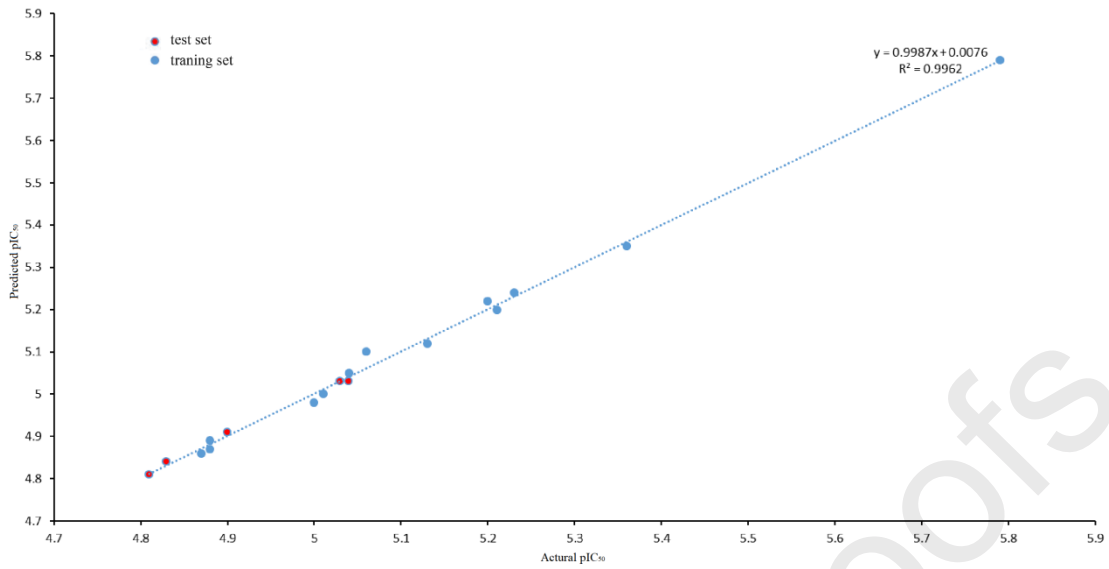

Fig. 10. Plot of experimental versus predicted anti-proliferative activities of training set and test set. The model was set up with correlation coefficient R^2 of 0.9962, which indicated that this model possessed pretty good predicting capability.

Moreover, the molecules aligned with the iso-surfaces of the 3D-QSAR model co-efficient on van der Waals grids and electrostatic potential grids were also listed in **Fig. 11**. Electrostatic map indicates red contours around regions where high electron density (negative charge) is expected to increase anti-proliferation activity, and blue contours represent areas where low electron density (partial positive charge) is expected to increase anti-proliferation activity. Similarly, steric map indicates green contours around areas where large steric bulk is predicted to increase activity and yellow contours around areas where small steric bulk is expected to decrease activity. The map predicted that the compounds that contained higher negative charge and bulky group such as F-substituted group in benzene ring would promote the anti-proliferation activity. This model was based on the actual experiments to guide and optimize the

tubulin and EGFR inhibitors for the future study.

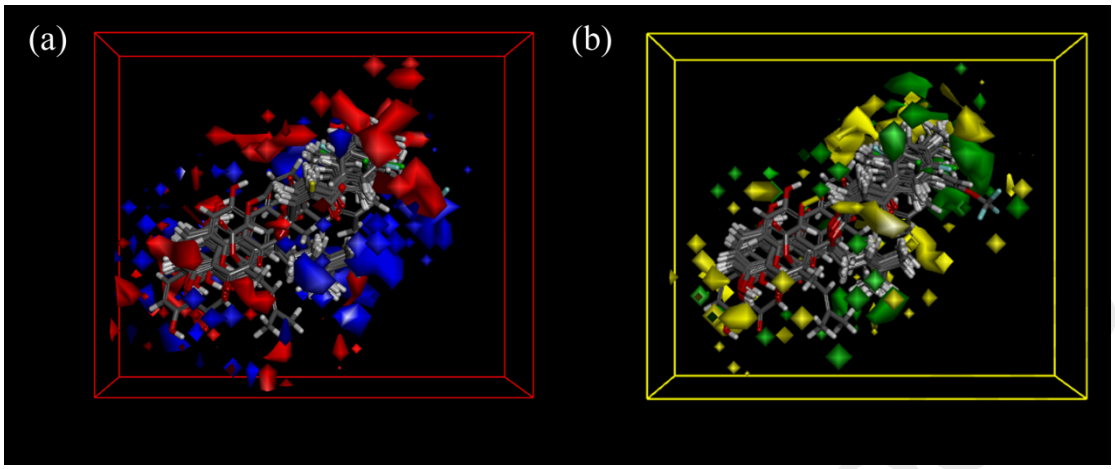

Fig. 11. (a) 3D-QSAR model coefficients on electrostatic potential grids. Blue represents positive coefficients; red represents negative coefficients. (b) 3D-QSAR model coefficients on van der Waals grids. Green represents positive coefficients; yellow represents negative coefficients.

3. Experiments Section

3.1. Materials and measurements

All chemicals reagents and solvents for the synthesis of the compounds were of analytical grade, purchased from Nanjing Chemical CO. Ltd (China) and used without further purification, unless otherwise specified. All the ^{1}H NMR spectra were recorded on a Bruker DPX 300 model spectrometer in $CDCl_3$. ^{13}C NMR spectra were recorded on a Bruker DPX 600 spectrometer in $CDCl_3$. Chemical shifts (δ) for ^{1}H NMR and ^{13}C NMR spectra were reported in ppm(δ), using TMS as an internal standard. ESI-MS spectra were obtained on a Mariner Biospectrometry Workstation (ESI-TOF) mass spectrometer. Melting points (uncorrected) were detected on a XT4 MP Apparatus (Taike Corp., Beijing, China), Thin layer chromatography (TLC) was carried out on glass-backed silica gel plates (Silica Gel 60 Å GF254) and visualized in UV light (λ 254 nm). Column chromatography was performed using silica gel (200-300 mesh) and eluting with ethyl acetate, dichloromethane and petroleum ether (bp 30-60 ℃).

MTT (methyl thiazolyl tetrazolium), PMSF (phenylmethanesulfonyl fluoride), DAPI (4',6-diamidino-2-phenylindole), RIPA lysis buffers (#P0013B), Anti-tubulin (#AT819), and Cy3-labeled goat anti-mouse IgG (H+L) (#A0521) were purchased from Beyotime Institute of Biotechnology (Haimen, China). BCA protein assay kit (#23227) was purchased from Pierce (Rockford, IL, USA). PVDF membranes were purchased from Thermo Scientific. JC-1 assay kit (#C2006) was purchased from Beyotime Institute of Biotechnology (Haimen, China). Anti-Axin-2 (20540-1-AP) was purchased from Proteintech (Wuhan, China); anti-cleaved PARP-1 (#sc-56196) was purchased

from Santa Cruz Biotechnology Inc. (Dallas, Texas, USA). anti-GAPDH (#5174) was purchased from Cell Signaling Technology (Beverly, MA). The secondary antibody (anti-mouse or anti-rabbit IgG) (#E1WP319 or #E1WP318) were purchased from Enogene (Nanjing, China). Anti-EGFR (WL03432), Anti-p-EGFR (WL03432), anti-Raf1 (WL00553), anti-Ras (WL0257), anti-PARP (WL01578), anti-Cleaved PARP (WL01932), anti-ERK1/2 (WL01864), anti-CDK1 (WL01718), anti-CDK2 (WL02028), anti-p-ERK1/2 (WLP1512), anti-Akt (WL0003b), anti-p-Akt (WLP001a), anti-CyclinA (WL01753), anti-Caspase-9 (WL03229), anti-PI3 Kinase p85 (WL02240), anti-Cleaved caspase-9 (WL01838), anti-Caspase-3 (WL01992a), anti-cleaved caspase-3 (WL02348), anti-*β*-actin (WL01372), anti-mTOR (WL02477), and anti-*β*-catenin (WL0962a) were purchased from Wanlei Biotech Co. Ltd (Shenyang, China), anti-Phospho-c-Raf (Ser338) (56A6) Rabbit mAb (#9427) and anti-Phospho-PI3 Kinase p85 (Tyr458)/p55 (Tyr199) were purchased from Cell Signaling Technology (Beverly, MA). The cell cycle and Annexin V-FITC cell apoptosis assay kits were purchased from KeyGEN Biotech Co. Ltd (Nanjing, China). ECL Kit (#34077) was purchased from Thermo Scientific (USA). Reactive Oxygen Species Assay Kit were purchased from YEASEN (Shanghai, China).

3.2. General procedure for the synthesis of compounds 2a-2o

All the synthesized compounds along with synthetic route were listed in **Scheme 1**. The catalyst 0.02 mol of anhydrous aluminum chloride and 0.01 mol maleic anhydride were dissolved in 40 mL flask, stirring at room temperature 10 min, the aluminum chloride anhydrous and maleic anhydride were fully dissolved. Then 0.01

mol xylene slowly added into solution, the color of the solution gradually turned tawny. The reaction system was stirred at 12 h at room temperature and monitored by TLC. After the reaction was completed, a dilute hydrochloric acid (*w/v* 20%) was added to the reaction system, followed by a 100 mL separation funnel for extraction separation three times. Take the lower dichloromethane solvent layer and mix with proper amount of anhydrous sodium sulfate to dry. The yellowish solid 2a of the rough intermediate product was obtained by evaporating the solvent under a rotary evaporator.

The obtained pale yellow intermediate is added to a saturated solution of 100 mL sodium bicarbonate and is constantly stirred until the solid dissolves completely. Subsequently, the solution pH=2 is adjusted with dilute hydrochloric acid, where the solution appears to be yellowish solid. Filtration and drying of solid pure yellow intermediate 2a. The synthesis, separation and purification methods of the intermediate product 2a are suitable for all intermediate product derivatives (2a-2o) (**Scheme 1**).

3.3. General procedure for the synthesis of compounds PMMB-311-PMMB-325

At room temperature, 50 mmol intermediate, benzoyl acrylic acid derivative (2a) was added to 30 mL anhydrous dichloromethane to make it fully dissolved. The catalyst dicyclohexylcarbodiimide (DCC) and 4-dimethylaminopyridine (DMAP) are added into the solution system by 0.1 times the amount of the intermediate, stirring 20 min. Add 25 mmol shikonin to the reaction solution and continue mixing 3-4 h. Progress of the reaction was monitored by the TLC. Finally, target compounds were collected by column chromatography **(Scheme 1**). Chemical structures of the target compounds (PMMB-311-PMMB-325) shown in **Table 1** and the eluent composition and proportion

are shown in **Table S**2 (***SI Appendix***). Theoretically, there may occur the geometrical isomerism of the double bonds in the target compounds. Although structural characterization through X-ray single crystal diffraction was difficult to be obtained, the TLC, HPLC detections and ^{1}H NMR assay have been conducted. During the TLC detection and HPLC analysis, there is only one new compound, which means only to be either *cis*- or *trans*- conformation. In theory, the *trans*- conformation is more reasonable due to its lower energy and more stablilty. Moreover, all ^{1}H NMR spectrums of the target compounds are in accordance to the *trans*- conformation. If they are *cis*-conformation, the carbonyl group must have an effect on the hydrogen displacement of side chain of shikonin. Apparently, all the ^{1}H NMR spectrums showed no such change in hydrogen displacement of side chain of shikonin. Thus, the combined results above indicated that the double bond exists in a more stable *trans*- conformation.

3.3.1. 1-(5,8-Dihydroxy-1,4-dioxo-1,4-dihydronaphthalen-2-yl)-4-methylpent-3-en-1-yl(Z)-4-(2,5-dimethylphenyl)-4-oxobut-2-enoate ***(PMMB-311)***

Red powder，Mp: 50.3-51.8 °C. Yield: 73%. ^{1}H NMR (300 MHz, $CDCl_3$) δ 12.61 (s, 1H, -OH), 12.42 (s, 1H, -OH), 7.64 (t, J = 11.9 Hz, 1H, -C-CH=C), 7.40 (d, J = 8.9 Hz, 1H, -C-CH=C), 7.24 (s, 1H, Ar-H), 7.21-7.14 (m, 3H, Ar-H), 7.02 (s, 1H, Ar-H), 6.76 (d, J = 15.7 Hz, 1H, -C-CH=C), 6.15 (dd, J = 6.7, 4.8 Hz, 1H, -O-CH-), 5.15 (t, J = 7.3 Hz, 1H, -C-CH=C), 2.75-2.49 (m, 2H, $-CH_2-$), 2.45 (s, 3H, Ar-CH), 2.36 (d, J = 11.1 Hz, 3H, Ar-CH), 1.70 (s, 3H, C=C-CH_3), 1.60 (s, 3H, C=C-CH_3). ^{13}C NMR (151 MHz, $CDCl_3$) δ 193.52 (s, 20C), 177.00 (s, 8C), 175.46 (s, 5C), 168.63 (s, 17C), 168.10 (s, 4C), 164.50 (s, 1C), 147.21 (s, 7C), 140.89 (s, 19C), 136.56 (s, 22C), 135.59 (s, 25C),

135.46 (s, 6C), 133.36 (s, 24C), 133.15 (s, 21C), 132.90 (s, 23C), 131.92 (s, 14C), 131.43 (s, 18C), 131.29 (s, 2C, 3C), 129.79 (s, 26C), 117.38 (s, 13C), 111.84 (s, 9C), 111.61 (s, 10C), 70.59 (s, 11C), 32.85 (s, 12C), 25.83 (s, 16C), 20.90 (s, 4' C), 20.45 (s, 15C), 18.04 (s, 1'C). ESI-TOF, calcd for $C_{28}H_{26}O_7$ ([M+Na]$^+$), 497.499, found 497.159. Anal. Calcd for $C_{28}H_{26}O_7$: C, 70.87; H, 5.52; O, 23.60; Found: C, 70.34; H, 5.42; O, 23.19.

3.3.2. 1-(5,8-Dihydroxy-1,4-dioxo-1,4-dihydronaphthalen-2-yl)-4-methylpent-3-en-1-yl (Z)-4-oxo-4-(p-tolyl)but-2-enoate ***(PMMB-312)***

Red powder，Mp: 51.8-53.5 °C. Yield: 56%. ^{1}H NMR (300 MHz, $CDCl_3$) δ 12.61 (d, J = 2.3 Hz, 1H, -OH), 12.41 (d, J = 2.4 Hz, 1H, -OH), 8.02-7.86 (m, 3H, Ar-H, -C-CH=C), 7.31 (t, J = 7.6 Hz, 2H, Ar-H), 7.18 (d, J = 8.7 Hz, 2H, Ar-H), 7.03 (t, J = 4.2 Hz, 1H, -C-CH=C), 6.94 (t, J = 10.3 Hz, 1H, -C-CH=C), 6.17 (dd, J = 6.4, 4.7 Hz, 1H, -O-CH-), 5.15 (t, J = 7.3 Hz, 1H, -C-CH=C), 2.77-2.49 (m, 3H, Ar-CH), 2.48-2.37 (m, 2H, -CH_2-), 1.70 (s, 3H, C=C-CH_3), 1.61 (s, 3H, C=C-CH_3). ^{13}C NMR (151 MHz, $CDCl_3$) δ 188.69 (s, 20C), 177.08 (s, 8C), 175.56 (s, 5C), 168.56 (s, 17C), 168.02 (s, 4C), 164.52 (s, 1C), 147.26 (s, 7C), 145.20 (s, 24C), 137.76 (s, 19C), 136.55 (s, 6C), 134.01 (s, 21C), 133.33 (s, 18C), 133.10 (s, 14C), 131.34 (s, 2C), 131.19 (s, 3C), 129.68 (s, 22C, 26C), 129.06 (s, 23C, 25C), 117.39 (s, 13C), 111.85 (s, 9C), 111.61 (s, 10C), 70.55 (s, 11C), 32.84 (s, 12C), 25.79 (s, 16C), 21.82 (s, 3'C), 18.02 (s, 15C). ESI-TOF, calcd for $C_{27}H_{24}O_7$ ([M+Na]$^+$), 483.469, found 483.140. Anal. Calcd for $C_{27}H_{24}O_7$: C, 70.43; H, 5.25; O, 24.32; Found: C, 70.34; H, 5.12; O, 24.19.

3.3.3. 1-(5,8-Dihydroxy-1,4-dioxo-1,4-dihydronaphthalen-2-yl)-4-methylpent-3-en-1-

yl (Z)-4-(3,4-dimethylphenyl)-4-oxobut-2-enoate ***(PMMB-313)***

Red powder，Mp: 48.7-48.9 °C. Yield: 45%. ^{1}H NMR (300 MHz, $CDCl_3$) δ 12.61 (d, J = 2.3 Hz, 1H, -OH), 12.41 (d, J = 2.4 Hz, 1H, -OH), 7.97 (d, J = 15.5 Hz, 1H, Ar-H), 7.82-7.69 (m, 2H, -C-CH=C), 7.28 (d, J = 7.2 Hz, 1H, Ar-H), 7.19 (s, 2H, Ar-H), 7.04 (d, J = 0.9 Hz, 1H, Ar-H), 6.95 (d, J = 15.5 Hz, 1H, -C-CH=C), 6.17 (dd, J = 6.4, 4.7 Hz, 1H, -O-CH-), 5.16 (t, J = 7.3 Hz, 1H, -C-CH=C), 2.79-2.47 (m, 2H, -CH_2-), 2.35 (s, 6H, Ar-CH), 1.70 (s, 3H, C=C-CH_3), 1.61 (s, 3H, C=C-CH_3). ^{13}C NMR (151 MHz, $CDCl_3$) δ 188.83 (s, 20C), 177.13 (s, 8C), 175.61 (s, 5C), 168.50 (s, 17C), 167.96 (s, 4C), 164.59 (s, 1C), 147.28 (s, 7C), 144.01 (s, 19C), 137.91 (s, 24C), 137.51 (s, 23C), 136.54 (s, 21C), 134.37 (s, 6C), 133.31 (s, 25C), 133.08 (s, 14C), 131.34 (s, 18C), 131.00 (s, 2C), 130.17 (s, 3C), 129.97 (s, 22C), 126.71 (s, 26C), 117.39 (s, 13C), 111.83 (s, 9C), 111.60 (s, 10C), 70.52 (s, 11C), 32.85 (s, 12C), 25.82 (s, 16C), 20.21 (s, 15C), 19.81 (s, 2'C), 18.03 (s, 3'C). ESI-TOF, calcd for $C_{28}H_{26}O_7$ ($[M+Na]^+$), 497.499, found 497.159. Anal. Calcd for $C_{28}H_{26}O_7$: C, 70.87; H, 5.52; O, 23.60; Found: C, 70.33; H, 5.45; O, 23.18.

3.3.4. 1-(5,8-Dihydroxy-1,4-dioxo-1,4-dihydronaphthalen-2-yl)-4-methylpent-3-en-1-yl (Z)-4-(2-chloro-4-methylphenyl)-4-oxobut-2-enoate ***(PMMB-314)***

Red oil，Yield: 58%. ^{1}H NMR (300 MHz, $CDCl_3$) δ 12.61 (s, 1H, -OH), 12.41 (s, 1H, -OH), 7.70-7.58 (m, 1H, -C-CH=C), 7.52 (dd, J = 20.1, 8.2 Hz, 1H, Ar-H), 7.33-7.26 (m, 2H, Ar-H, -C-CH=C), 7.19 (s, 2H, Ar-H), 7.01 (d, J = 0.8 Hz, 1H, Ar-H), 6.76 (dd, J = 15.7, 1.6 Hz, 1H, -C-CH=C), 6.15 (dd, J = 6.5, 4.8 Hz, 1H, -O-CH-), 5.14 (t, J = 7.3 Hz, 1H, -C-CH=C), 2.75-2.53 (m, 2H, -CH_2-), 2.45 (d, J = 27.0 Hz, 3H, Ar-CH),

1.70 (s, 3H, C=C-CH_3), 1.59 (s, 3H, C=C-CH_3). ^{13}C NMR (151 MHz, $CDCl_3$) δ 192.18 (s, 20C), 176.72 (s, 8C), 175.16 (s, 5C), 168.86 (s, 17C), 168.33 (s, 4C), 164.25 (s, 1C), 147.02 (s, 7C), 141.02 (s, 24C), 140.28 (s, 19C), 138.21 (s, 6C), 136.59 (s, 22C), 134.86 (s, 21C), 133.44 (s, 14C), 133.23 (s, 18C), 132.05 (s, 26C), 131.94 (s, 2C), 131.19 (s, 3C), 130.68 (s, 23C), 126.03 (s, 25C), 117.28 (s, 13C), 111.81 (s, 9C), 111.58 (s, 10C), 70.69 (s, 11C), 32.80 (s, 12C), 25.80 (s, 16C), 20.85 (s, 3'C), 18.01 (s, 15C). ESI-TOF, calcd for $C_{27}H_{23}ClO_7$ ([M+Na]$^+$), 517.909, found 517.101. Anal. Calcd for $C_{27}H_{23}ClO_7$: C, 65.52; H, 4.68; Cl, 7.16; O, 22.63; Found: C, 65.34; H, 4.62; Cl, 7.18; O, 21.61.

3.3.5. 1-(5,8-Dihydroxy-1,4-dioxo-1,4-dihydronaphthalen-2-yl)-4-methylpent-3-en-1-yl (Z)-4-(4-ethylphenyl)-4-oxobut-2-enoate ***(PMMB-315)***

Red powder，Mp: 56.8-57.2 °C. Yield: 64%. ^{1}H NMR (300 MHz, $CDCl_3$) δ 12.61 (s, 1H, -OH), 12.41 (s, 1H, -OH), 7.95 (dd, J = 11.9, 7.4 Hz, 3H, Ar-H, -C-CH=C), 7.35 (d, J = 8.1 Hz, 2H, Ar-H), 7.19 (s, 2H, Ar-H), 7.04 (s, 1H, -C-CH=C), 6.95 (d, J = 15.5 Hz, 1H, -C-CH=C), 6.17 (dd, J = 7.1, 4.6 Hz, 1H, -O-CH-), 5.16 (t, J = 7.2 Hz, 1H, -C-CH=C), 2.79-2.71 (m, 2H, Ar-CH_2-), 2.70-2.50 (m, 2H, -CH_2-), 1.70 (s, 3H, C=C-CH_3), 1.61 (s, 3H, C=C-CH_3), 1.25-1.23 (m, 3H, -C-CH_3). ^{13}C NMR (151 MHz, $CDCl_3$) δ 188.72 (s, 20C), 177.08 (s, 8C), 175.56 (s, 5C), 168.56 (s, 17C), 168.02 (s, 4C), 164.52 (s, 1C), 151.33 (s, 24C), 147.26 (s, 7C), 137.79 (s, 19C), 136.55 (s, 6C), 134.21 (s, 21C), 133.33 (s, 18C), 133.10 (s, 14C), 131.34 (s, 2C), 131.17 (s, 3C), 129.17 (s, 22C, 26C), 128.51 (s, 23C, 25C), 117.39 (s, 13C), 111.85 (s, 9C), 111.61 (s, 10C), 70.55 (s, 11C), 32.86 (s, 12C), 29.05 (s, 3'C), 25.81 (s, 16C), 18.02 (s, 15C), 15.12 (s, 3''C). ESI-TOF, calcd for $C_{28}H_{26}O_7$ ([M+Na]$^+$), 497.499, found 497.157. Anal. Calcd for

$C_{28}H_{26}O_7$: C, 70.87; H, 5.52; O, 23.60; Found: C, 70.34; H, 5.42; O, 23.18.

3.3.6. 1-(5,8-Dihydroxy-1,4-dioxo-1,4-dihydronaphthalen-2-yl)-4-methylpent-3-en-1-yl (Z)-4-(4-chlorophenyl)-4-oxobut-2-enoate ***(PMMB-316)***

Red oil，Yield: 45%. ^{1}H NMR (300 MHz, $CDCl_3$) δ 12.62 (s, 1H, -OH), 12.41 (s, 1H, -OH), 7.93 (t, J = 11.9 Hz, 3H, Ar-H, -C-CH=C), 7.49 (dd, J = 12.8, 11.0 Hz, 2H, Ar-H), 7.19 (s, 2H, Ar-H), 7.00 (dd, J = 18.2, 8.2 Hz, 2H), 6.17 (dd, J = 6.7, 4.9 Hz, 1H, -O-CH-), 5.15 (s, 1H, -C-CH=C), 2.77-2.47 (m, 2H, -CH_2-), 1.70 (s, 3H, C=C-CH_3), 1.61 (s, 3H, C=C-CH_3). ^{13}C NMR (151 MHz, $CDCl_3$) δ 187.93 (s, 20C), 176.79 (s, 8C), 175.25 (s, 5C), 168.82 (s, 17C), 168.28 (s, 4C), 164.28 (s, 1C), 147.05 (s, 7C), 140.69 (s, 19C), 136.96 (s, 24C), 136.60 (s, 21C), 134.75 (s, 6C), 133.43 (s, 2C), 133.21 (s, 3C), 132.01 (s, 22C), 131.25 (s, 26C), 130.24 (s, 25C), 129.34 (s, 23C), 117.32 (s, 13C), 111.83 (s, 9C), 111.60 (s, 10C), 70.71 (s, 11C), 32.83 (s, 12C), 25.82 (s, 16C), 18.03 (s, 15C). ESI-TOF, calcd for $C_{26}H_{21}ClO_7$ ([M+Na]$^+$), 503.889, found 503.089. Anal. Calcd for $C_{26}H_{21}ClO_7$: C, 64.94; H, 4.40; Cl, 7.37; O, 23.29; Found: C, 64.74; H, 4.52; Cl, 7.21; O, 22.89.

3.3.7. *1-(5,8-Dihydroxy-1,4-dioxo-1,4-dihydronaphthalen-2-yl)-4-methylpent-3-en-1-yl (Z)-4-(4-fluorophenyl)-4-oxobut-2-enoate* ***(PMMB-317)***

Red powder，Mp: 56.4-57.5 °C. Yield: 68%. ^{1}H NMR (300 MHz, $CDCl_3$) δ 12.61 (d, J = 2.3 Hz, 1H, -OH), 12.41 (d, J = 2.4 Hz, 1H, -OH), 8.10-7.99 (m, 2H, Ar-H), 7.93 (d, J = 15.5 Hz, 1H, -C-CH=C), 7.25-7.21 (m, 1H, -C-CH=C), 7.21-7.14 (m, 3H, Ar-H), 7.04 (d, J = 0.9 Hz, 1H, Ar-H), 6.95 (t, J = 12.6 Hz, 1H, -C-CH=C), 6.23-6.11 (m, 1H, -O-CH-), 5.15 (t, J = 7.3 Hz, 1H, -C-CH=C), 2.79-2.44 (m, 2H, -CH_2-), 1.70 (s,

3H, C=C-CH_3), 1.61 (s, 3H, C=C-CH_3). ^{13}C NMR (151 MHz, $CDCl_3$) δ 187.54 (s, 20C), 176.82 (s, 8C), 175.29 (s, 5C), 168.81 (s, 24C), 168.27 (s, 17C), 165.46 – 165.45 (m, 4C), 164.33 (s, 1C), 147.09 (s, 7C), 137.87 (s, 19C), 136.60 (s, 6C), 133.43 (s, 21C), 133.21 (s, 18C), 132.88 (s, 14C),131.77 (s, 22C), 131.68 (s, 26C), 131.61 (s, 2C), 131.26 (s, 3C), 117.33 (s, 13C), 116.32 (s, 23C), 116.17 (s, 25C), 111.84 (s, 9C), 111.61 (s, 10C), 70.69 (s, 11C), 32.84 (s, 12C), 25.81 (s, 16C), 18.02 (s, 15C). ESI-TOF, calcd for $C_{26}H_{21}FO_7$ ([M+Na]$^+$), 487.439, found 487.116. Anal. Calcd for $C_{26}H_{21}FO_7$: C, 67.24; H, 4.56; F, 4.09; O, 24.11; Found: C, 67.04; H, 4.54; F, 4.29; O, 24.10.

3.3.8. 1-(5,8-Dihydroxy-1,4-dioxo-1,4-dihydronaphthalen-2-yl)-4-methylpent-3-en-1-yl (Z)-4-(2-fluoro-4-methylphenyl)-4-oxobut-2-enoate ***(PMMB-318)***

Red powder，Mp: 46.3-46.9 °C. Yield: 43%. ^{1}H NMR (300 MHz, $CDCl_3$) δ 12.61 (d, J = 2.3 Hz, 1H, -OH), 12.41 (d, J = 2.4 Hz, 1H, -OH), 7.99-7.79 (m, 3H, Ar-H, -C-CH=C), 7.19 (s, 2H, Ar-H), 7.14 (t, J = 8.8 Hz, 1H, Ar-H), 7.04 (d, J = 0.9 Hz, 1H, Ar-H), 6.94 (t, J = 11.1 Hz, 1H, -C-CH=C), 6.17 (dd, J = 6.5, 4.7 Hz, 1H, -O-CH-), 5.15 (t, J = 7.3 Hz, 1H, -C-CH=C), 2.89-2.44 (m, 2H, -CH_2-), 2.34 (t, J = 7.4 Hz, 3H, Ar-CH), 1.70 (s, 3H, C=C-CH_3), 1.61 (s, 3H, C=C-CH_3). ^{13}C NMR (151 MHz, $CDCl_3$) δ 187.73 (s, 20C), 176.90 (s, 8C), 175.37 (s, 5C), 168.72 (s, 17C), 168.19 (s, 4C), 164.42 (s, 23C), 147.14 (s, 1C), 137.36 (s, 7C), 136.58 (s, 19C), 133.40 (s, 21C), 133.18 (s, 6C), 132.80 (s, 14C), 132.75 (s, 18C), 132.60 (s, 25C), 132.58 (s, 2C), 131.52 (s, 3C), 131.28 (s, 24C), 129.02 (s, 26C), 126.16 (s, 13C), 117.35 (s, 22C), 115.67 (s, 9C), 111.60 (s, 10C), 70.65 (s, 11C), 32.83 (s, 12C), 25.82 (s, 16C), 18.03 (s, 15C), 14.63 (s, 3'C). ESI-TOF, calcd for $C_{27}H_{23}FO_7$ ([M+Na]$^+$), 501.459, found 501.132. Anal.

Calcd for $C_{27}H_{23}FO_7$: C, 67.78; H, 4.85; F, 3.97; O, 23.41; Found: C, 67.74; H, 4.64; F, 3.96; O, 23.52.

3.3.9. 1-(5,8-Dihydroxy-1,4-dioxo-1,4-dihydronaphthalen-2-yl)-4-methylpent-3-en-1-yl (Z)-4-(2,4-dimethylphenyl)-4-oxobut-2-enoate ***(PMMB-319)***

Red powder，Mp: 51.1-52.4 °C. Yield: 73%. ^{1}H NMR (300 MHz, $CDCl_3$) δ 12.61 (d, J = 2.3 Hz, 1H, -OH), 12.41 (d, J = 2.4 Hz, 1H, -OH), 7.97 (d, J = 15.5 Hz, 1H, -C=CH), 7.75 (dd, J = 12.8, 4.9 Hz, 2H, Ar-H, -C-CH=C), 7.29 (s, 1H, Ar-H), 7.19 (s, 2H, Ar-H), 7.04 (d, J = 0.9 Hz, 1H, Ar-H), 6.95 (d, J = 15.5 Hz, 1H, -C-CH=C), 6.17 (dd, J = 6.4, 4.7 Hz, 1H, -O-CH-), 5.16 (t, J = 7.3 Hz, 1H, -C-CH=C), 2.79-2.44 (m, 2H, $-CH_2-$), 2.35 (s, 6H, Ar-CH), 1.70 (s, 3H, C=C-CH_3), 1.61 (s, 3H, C=C-CH_3). ^{13}C NMR (151 MHz, $CDCl_3$) δ 192.55 (s, 20C), 177.07 (s, 8C), 175.53 (s, 5C), 168.53 (s, 17C), 168.00 (s, 4C), 164.50 (s, 1C), 147.25 (s, 7C), 143.06 (s, 19C), 140.91 (s, 24C), 139.38 (s, 22C), 136.53 (s, 6C), 133.74 (s, 18C), 133.31 (s, 14C), 133.10 (s, 23C), 132.97 (s, 21C), 131.28 (s, 2C), 131.05 (s, 3C), 129.95 (s, 26C), 126.44 (s, 25C), 117.35 (s, 13C), 111.82 (s, 9C), 111.59 (s, 10C), 70.51 (s, 11C), 32.82 (s, 12C), 25.80 (s, 16C), 21.51 (s, 3'C), 21.14 (s, 15C), 18.01 (s, 1'C). ESI-TOF, calcd for $C_{28}H_{26}O_7$ ($[M+Na]^+$), 497.499, found 497.156. Anal. Calcd for $C_{28}H_{26}O_7$: C, 70.87; H, 5.52; O, 23.60; Found: C, 70.33; H, 5.43; O, 23.17.

3.3.10. 1-(5,8-Dihydroxy-1,4-dioxo-1,4-dihydronaphthalen-2-yl)-4-methylpent-3-en-1-yl(Z)-4-(3-bromo-4-methylphenyl)-4-oxobut-2-enoate ***(PMMB-320)***

Red powder，Mp: 46.9-48.1 °C. Yield: 70%. ^{1}H NMR (300 MHz, $CDCl_3$) δ 12.62 (s, 1H, -OH), 12.41 (s, 1H, -OH), 7.97-7.78 (m, 2H, Ar-H), 7.74-7.33 (m, 2H, -C-

CH=C), 7.19 (s, 2H, Ar-H), 7.07-6.89 (m, 2H, Ar-H, -C-CH=C), 6.17 (dd, J = 6.7, 4.9 Hz, 1H, -O-CH-), 5.15 (t, J = 7.4 Hz, 1H, -C-CH=C), 2.79-2.52 (m, 2H, -CH_2-), 2.46 (d, J = 18.4 Hz, 3H, Ar-CH), 1.70 (s, 3H, C=C-CH_3), 1.61 (s, 3H, C=C-CH_3). ^{13}C NMR (151 MHz, $CDCl_3$) δ 188.36 (s, 20C), 176.80 (s, 8C), 175.27 (s, 5C), 168.79 (s, 17C), 168.25 (s, 4C), 164.35 (s, 1C), 147.07 (s, 7C), 139.09 (s, 24C), 137.14 (s, 19C), 136.59 (s, 21C), 135.44 (s, 6C), 133.42 (s, 22C), 133.20 (s, 25C), 133.08 (s, 14C), 131.93 (s, 18C), 131.82 (s, 2C), 131.25 (s, 3C), 130.83 (s, 26C), 127.50 (s, 23C), 117.32 (s, 13C), 111.82 (s, 9C), 111.59 (s, 10C), 70.68 (s, 11C), 32.81 (s, 12C), 25.81 (s, 16C), 23.02 (s, 3'C), 18.02 (s, 15C). ESI-TOF, calcd for $C_{27}H_{23}BrO_7$ ([M+Na]$^+$), 562.369, found 561.049. Anal. Calcd for $C_{27}H_{23}BrO_7$: C, 60.12; H, 4.30; Br, 14.81; O, 20.76; Found: C, 60.14; H, 4.26; Br, 14.84; O, 20.61.

3.3.11. 1-(5,8-Dihydroxy-1,4-dioxo-1,4-dihydronaphthalen-2-yl)-4-methylpent-3-en-1-yl (Z)-4-(5-chloro-2-methylphenyl)-4-oxobut-2-enoate ***(PMMB-321)***

Red powder， Mp: 53.6-54.2 °C. Yield: 63%. 1H NMR (300 MHz, $CDCl_3$) δ 12.60 (d, J = 2.2 Hz, 1H, -OH), 12.41 (s, 1H, -OH), 7.70-7.45 (m, 2H, Ar-H, -C-CH=C), 7.30 (dd, J = 8.7, 1.6 Hz, 2H, -C-CH=C, Ar-H), 7.19 (s, 2H, Ar-H), 7.03 (t, J = 5.8 Hz, 1H, Ar-H), 6.76 (dd, J = 15.7, 1.7 Hz, 1H, -C-CH=C), 6.15 (dd, J = 6.4, 4.7 Hz, 1H, -O-CH-), 5.14 (t, J = 7.3 Hz, 1H, -C-CH=C), 2.63 (ddd, J = 22.3, 15.0, 8.3 Hz, 2H, -CH_2-), 2.45 (d, J = 27.0 Hz, 3H, Ar-CH), 1.70 (s, 3H, C=C-CH_3), 1.59 (s, 3H, C=C-CH_3). ^{13}C NMR (151 MHz, $CDCl_3$) δ 192.40 (s, 20C), 176.69 (s, 8C), 175.14 (s, 5C), 168.91 (s, 17C), 168.38 (s, 4C), 164.15 (s, 1C), 146.97 (s, 7C), 140.01 (s, 19C), 138.03 (s, 22C), 136.80 (s, 21C), 136.64 (s, 6C), 133.62 (s, 24C), 133.29 (s, 14C), 133.25 (s,

18C), 132.43 (s, 25C), 131.89 (s, 23C), 130.46 (s, 2C), 130.37 (s, 3C), 128.79 (s, 26C), 117.28 (s, 13C), 111.82 (s, 9C), 111.60 (s, 10C), 70.75 (s, 11C), 32.81 (s, 12C), 25.82 (s, 16C), 20.21 (s, 1'C), 18.03 (s, 15C). ESI-TOF, calcd for $C_{27}H_{23}ClO_7$ ([M+Na]$^+$), 517.909, found 517.102. Anal. Calcd for $C_{27}H_{23}ClO_7$: C, 65.52; H, 4.68; Cl, 7.16; O, 22.63; Found: C, 65.46; H, 4.55; Cl, 7.18; O, 22.53.

3.3.12. 1-(5,8-Dihydroxy-1,4-dioxo-1,4-dihydronaphthalen-2-yl)-4-methylpent-3-en-1-yl (Z)-4-oxo-4-phenylbut-2-enoate ***(PMMB-322)***

Red powder，Mp: 59.3-60.1 °C. Yield: 55%. ^{1}H NMR (300 MHz, $CDCl_3$) δ 12.62 (s, 1H, -OH), 12.42 (s, 1H, -OH), 7.98 (dd, J = 13.3, 11.5 Hz, 3H, Ar-H, -C-CH=C), 7.70-7.59 (m, 1H, -C-CH=C), 7.53 (t, J = 7.5 Hz, 2H, Ar-H), 7.18 (d, J = 9.0 Hz, 2H, Ar-H), 7.04 (s, 1H, Ar-H), 6.95 (t, J = 12.3 Hz, 1H, -C-CH=C), 6.17 (dd, J = 6.7, 4.8 Hz, 1H, -O-CH-), 5.16 (t, J = 7.2 Hz, 1H, -C-CH=C), 2.79-2.46 (m, 2H, -CH_2-), 1.71 (s, 3H, C=C-CH_3), 1.61 (s, 3H, C=C-CH_3). ^{13}C NMR (151 MHz, $CDCl_3$) δ 189.23 (s, 20C), 177.02 (s, 8C), 175.49 (s, 5C), 168.62 (s, 17C), 168.08 (s, 4C), 164.43 (s, 1C), 147.20 (s, 7C), 137.57 (s, 19C), 136.59 (s, 21C), 136.45 (s, 6C), 134.06 (s, 24C), 133.37 (s, 14C), 133.14 (s, 18C), 131.58 (s, 2C, 3C), 131.32 (s, 23C, 25C), 128.99 (s, 22C), 128.91 (s, 26C), 117.39 (s 13C), 111.85 (s, 9C), 111.61 (s, 10C), 70.62 (s, 11C), 32.86 (s, 12C), 25.78 (s, 16C), 18.05 (s, 15C). ESI-TOF, calcd for $C_{26}H_{22}O_7$ ([M+Na]$^+$), 469.449, found 469.126. Anal. Calcd for $C_{26}H_{22}O_7$: C, 69.95; H, 4.97; O, 25.05; Found: C, 69.80; H, 4.85; O, 25.01.

3.3.13. 1-(5,8-Dihydroxy-1,4-dioxo-1,4-dihydronaphthalen-2-yl)-4-methylpent-3-en-1-yl (Z)-4-(2-fluoro-4-methylphenyl)-4-oxobut-2-enoate ***(PMMB-323)***

Red oil，Yield: 64%. ^{1}H NMR (300 MHz, $CDCl_3$) δ 12.60 (s, 1H, -OH), 12.41 (d, J = 1.6 Hz, 1H, -OH), 7.74-7.55 (m, 2H, Ar-H, -C-CH=C), 7.19 (s, 2H, Ar-H, -C-CH=C), 7.09-6.93 (m, 3H, Ar-H), 6.77 (d, J = 15.7 Hz, 1H, -C-CH=C), 6.15 (dd, J = 6.7, 5.1 Hz, 1H, -O-CH-), 5.14 (t, J = 7.3 Hz, 1H, -C-CH=C), 2.65 (ddd, J = 28.8, 14.9, 6.5 Hz, 2H, -CH_2-), 2.52 (d, J = 7.7 Hz, 3H, Ar-CH), 1.70 (s, 3H, C=C-CH_3), 1.60 (s, 3H, C=C-CH_3). ^{13}C NMR (151 MHz, $CDCl_3$) δ 191.65 (s, 20C), 176.83 (s, 8C), 175.28 (s, 5C), 168.77 (s, 17C), 168.24 (s, 4C), 164.32 (s, 22C), 147.10 (s, 1C), 142.97 (s, 7C), 140.46 (s, 24C), 136.58 (s, 19C), 133.41 (s, 6C), 133.20 (s, 14C), 132.11 (s, 18C), 132.05 (s, 26C), 131.61 (s, 2C), 131.22 (s, 3C), 119.13 (s, 25C), 118.99 (s, 13C), 117.32 (s, 21C), 112.79 (s, 23C), 111.82 (s, 9C), 111.59 (s, 10C), 70.66 (s, 11C), 32.82 (s, 12C), 25.81 (s, 16C), 21.28 (s, 3'C), 18.02 (s, 15C). ESI-TOF, calcd for $C_{27}H_{23}FO_7$ ($[M+Na]^+$), 501.459, found 501.132. Anal. Calcd for $C_{27}H_{23}FO_7$: C, 67.78; H, 4.85; F, 3.97; O, 23.41; Found: C, 67.79; H, 4.64; F, 3.99; O, 23.34.

3.3.14. 1-(5,8-Dihydroxy-1,4-dioxo-1,4-dihydronaphthalen-2-yl)-4-methylpent-3-en-1-yl (Z)-4-(5-fluoro-2-methylphenyl)-4-oxobut-2-enoate ***(PMMB-324)***

Red powder，Mp: 61.2-62.4 °C. Yield: 73%. ^{1}H NMR (300 MHz, $CDCl_3$) δ 12.60 (s, 1H, -OH), 12.41 (d, J = 2.1 Hz, 1H, -OH), 7.82 (dd, J = 15.6, 3.4 Hz, 1H, -C-CH=C), 7.61 (ddd, J = 18.8, 13.5, 8.3 Hz, 1H, -C-CH=C), 7.37 (ddd, J = 14.7, 8.2, 6.0 Hz, 1H, Ar-H), 7.22-7.15 (m, 2H, Ar-H), 7.13-6.99 (m, 2H, Ar-H), 6.96-6.83 (m, 1H, -C-CH=C), 6.16 (dd, J = 6.4, 4.6 Hz, 1H, -O-CH-), 5.15 (s, 1H, -C-CH=C), 2.79-2.50 (m, 2H, -CH_2-), 2.43-2.29 (m, 3H, Ar-CH), 1.70 (s, 3H, C=C-CH_3), 1.60 (s, 3H, C=C-CH_3). ^{13}C NMR (151 MHz, $CDCl_3$) δ 187.85 (s, 20C), 177.14 (s, 8C), 175.60 (s, 5C), 168.48

(s, 17C), 167.95 (s, 4C), 164.31 (s, 25C), 161.03 (s, 1C), 147.29 (s, 7C), 140.34 (s, 19C), 136.58 (s, 21C), 136.15 (s, 22C), 136.10 (s, 6C), 133.46 (s, 14C), 133.30 (s, 18C), 133.08 (s, 23C), 131.32 (s, 2C), 131.03 (s, 3C), 117.34 (s, 13C), 116.66 (s, 24C), 116.51 (s, 26C), 111.83 (s, 9C), 111.60 (s, 10C), 70.51 (s, 11C), 32.84 (s, 12C), 25.80 (s, 16C), 20.52 (s, 1'C), 17.99 (s, 15C). ESI-TOF, calcd for $C_{27}H_{23}FO_7$ ([M+Na]$^+$), 501.459, found 501.132. Anal. Calcd for $C_{27}H_{23}FO_7$: C, 67.78; H, 4.85; F, 3.97; O, 23.41; Found: C, 67.79; H, 4.64; F, 3.99; O, 23.32.

3.3.15. 1-(5,8-Dihydroxy-1,4-dioxo-1,4-dihydronaphthalen-2-yl)-4-methylpent-3-en-1-yl (Z)-4-(4-bromophenyl)-4-oxobut-2-enoate ***(PMMB-325).***

Red oil，Yield: 62%. ^{1}H NMR (300 MHz, $CDCl_3$) δ 12.61 (s, 1H, -OH), 12.41 (s, 1H, -OH), 7.89 (dd, J = 12.1, 9.5 Hz, 3H, Ar-H, -C-CH=C), 7.73-7.53 (m, 2H, Ar-H), 7.19 (s, 2H, Ar-H), 7.03 (d, J = 0.8 Hz, 1H, -C-CH=C), 6.97 (d, J = 15.5 Hz, 1H, -C-CH=C), 6.17 (dd, J = 6.4, 4.6 Hz, 1H, -O-CH-), 5.14 (d, J = 7.4 Hz, 1H, -C-CH=C), 2.79-2.49 (m, 2H, -CH_2-), 1.70 (s, 3H, C=C-CH_3), 1.61 (s, 3H, C=C-CH_3). ^{13}C NMR (151 MHz, $CDCl_3$) δ 188.16 (s, 20C), 176.76 (s, 8C), 175.22 (s, 5C), 168.85 (s, 17C), 168.31 (s, 4C), 164.28 (s, 1C), 147.04 (s, 7C), 136.92 (s, 19C), 136.61 (s, 21C), 135.15 (s, 6C), 133.45 (s, 23C, 25C), 133.23 (s, 14C), 132.35 (s, 18C), 132.05 (s, 2C), 131.24 (s, 3C), 130.31 (s, 22C, 26C), 129.49 (s, 24C), 117.31 (s, 13C), 111.83 (s, 9C), 111.60 (s, 10C), 70.72 (s, 11C, 1C), 32.83 (s, 12C), 25.82 (s, 16C), 18.03 (s, 15C). ESI-TOF, calcd for $C_{26}H_{21}BrO_7$ ([M+Na]$^+$), 548.339, found 547.039. Anal. Calcd for $C_{26}H_{21}BrO_7$: C, 59.44; H, 4.03; Br, 15.21; O, 21.32; Found: C, 58.42; H, 4.15; Br, 15.20; O, 20.52.

3.4. Methods

3.4.1. Cell lines and culture conditions

The cell lines used in this study were human lung cancer cell line (H460), human breast cancer cell line (MCF-7), carcinoma of cervix cell line (HeLa), human lung adenocarcinoma epithelial cell line (A549), human non-small cell lung cancer cell lines (NCI H1975) and human liver cell (L02). They were obtained from State Key Laboratory of Pharmaceutical Biotechnology, Nanjing University. Cells were maintained in DMEM (Hyclone) and H1975 were cultured in 1640 (Hyclone, China) supplemented with 10% fetal bovine serum (FBS; Gibico, USA), L-glutamine, and penicillin/streptomycin and incubated at 37 °C in humidified atmosphere containing 5% CO_2.

3.4.2. Animals feeding

BALB/C female nude mice (5-6 weeks old) were obtained from Beijing Vital River Laboratory Animal Technology Co., Ltd. Briefly, mice were fed with free access to pellet food and water in plastic cages at 21 ± 2 °C and kept on a 12 h light-dark cycle. All animal procedures were performed in accordance with the Guidelines for Care and Use of Laboratory Animals of Nanjing University and approved by the Animal Ethics Committee of the Ministry of Science and Technology of China (2006). All efforts were made to minimize animal's suffering and to reduce the number of animals used.

3.4.3. Anti-proliferation assay

The anti-proliferation assay of the prepared compounds against Hela, A549, H1975, H460, MCF-7 and non-tumorigenic L02 cell lines were evaluated using a standard (MTT)-based colorimetric assay with some modification. Cell lines were

grown to log phase in DMEM supplemented with 10% fetal bovine serum. Cell suspensions were prepared and 100 μL/well dispensed into 96-well plates giving 10^4 cells/well. The subsequent incubation was permitted at 37 °C, 5% CO_2 atmosphere overnight to allow the cells to reattach. Subsequently, cells were treated with the target compounds at increasing concentrations (0.1, 1, 10 and 100 μM) in the presence of 10% FBS for 24 h. Then, cell viability was assessed by the conventional 3-(4, 5-dimethylthiazol 2-yl)-2, 5-diphenyltetrazolium bromide (MTT) reduction assay and carried out strictly according to the manufacturer instructions. The absorbance (OD_{570}) was read on an ELISA reader (EPOCH, BioTek, USA). Afatinib was used as a positive drug[25, 26]. The IC_{50} values were exhibited in means SD of three independent experiments and showed in **Table 2**.

3.4.4. EGFR kinase phosphorylation assay

The assays were carried out as described previously[27, 28]. Phosphorylation assays were performed in a final volume of 20 μL containing 8 mM MOPS (pH 7.0), 0.2 mM EDTA, 10 mM $MnCl_2$, 200 μM substrate peptide, 0.25 mM DTT, 0.1 mg mL^{-1} BSA, 10 ng of wild-type EGFR kinase (catalogue no. 40187, BPS Bioscience), 10 mM magnesium acetate, 100 μM γ-[^{32}P] ATP, and inhibitors or DMSO control (1.25% v/v). For IC_{50} curves with the wild-type enzyme, the following concentrations of the compounds were tested in triplicate: 150, 100, 50, 25, 15, 10, 7.5, 5, and 2.5 nM. Reactions were started by the addition of the magnesium acetate/ATP mixture. After 30 min incubation at 30 ℃, 5 μL of each reaction was spotted on phosphocellulose P81 paper (Whatman). The P81 paper was then washed 5 times with 50 mM phosphoric acid for 15 min, dried, and exposed to a phosphorimager screen (Storm, GE Healthcare),

which was scanned and densitometrically analyzed the next day. The sequence of the substrate peptide was derived from phospholipase C-γ1. The IC_{50} values were calculated using nonlinear regression with normalized dose response fit using Prism GraphPad software.

3.4.5. Apoptosis analysis by flow cytometry

Apoptosis was measured by Annexin V-FITC/PI (KeyGEN Biotech Co. Ltd, China) double staining by flow cytometry. Briefly, 5.0×10^3 cells A549 cells were seeded in 6-well plates per well at 37 °C, 5 % CO_2 overnight, atmosphere and then treated with PMMB-317 at 0, 2, 4, 8 and 12 μM for 24 h in the dose-dependent test. For the time-dependent experiment, the adhered cells were incubated with compound PMMB-317 at 8 μM for 0, 12, 24, and 36 h. After that, the cells were harvested and washed with PBS and then cells were collected and washed twice with PBS and stained with 5 μL Annexin V-FITC and 5 μL PI in binding buffer for 15 min at room temperature in the dark. The Apoptotic cells were measured by a BD Accuri C6 Flowjo Cytometer (BD, USA). Data analysis was done using Flowjo 7.6.1 software and the percentage of cells for the lower right quadrant was used for statistics analysis using Graphpad prism 5.

3.4.6. Mitochondrial membrane potential (ΔΨm) staining

MMP was examined using a Mitochondrial Membrane Potential Assay Kit (Beyotime Institute of Biotechnology, Haimen, China) with a widely used fluorescent probe JC-1 (5,5′,6,6′-Tetrachloro-1,1′,3,3′-tetraethyl-imidacarbocyanine). According to the requirements, 5.0×10^4 cells (per well) were cultured in 6-well plates overnight and

then treated with PMMB-317 at 0, 2, 4 , 8 μM for 24 h in the dose-dependent test, also with positive control drug CCCP in another well for 20 min at 37 °C. Cells in all wells were collected and washed with PBS. Then 1 mL JC-1 staining solution (5 ×) was added to each EP tube and incubated at 37 °C for 30 min. Finally, cells were washed twice with JC-1 staining solution (1 ×) and then resuspended to detect by BD Accuri C6 Flowjo Cytometer and Olympus confocal microscope, and data was analyzed using FV-10-ASW 1.7 viewer.

3.4.7. Cell cycle analysis

Targeted cells (A549) cells were plated in 6-well plates (5.0×10^4 cells per well) and incubated at 37 °C for 12 h. Exponentially growing cells were then incubated with the PMMB-317 at 0, 2, 4 and 8 μM for 24 h., For the time-dependent experiment, the adhered cells were incubated with compound PMMB-317 at 8 μM for 0, 12, 24, and 36 h. Untreated cells (control) or cells treated with compound PMMB-317 were centrifuged with (2000 rpm at 4 °C for 10 min) and fixed in 70% ethanol at -20 °C for at least 12 h and subsequently resuspended in PBS containing 0.1 mg mL^{-1} RNase A and 5 μg mL^{-1} propidium iodide (PI). Cellular DNA content, for cell cycle distribution analysis was measured by flow cytometry (BD FACS Calibur, USA) plotting at least 10,000 events per sample. The percentage of cells in the G0/G1, S and G2/M phases of the cell cycle was determined using FlowJo 7.6 software.

3.4.8. Confocal microscopy assay

A549 cells were plated in glass bottom cell culture dish properly and incubated with 4, 8 μM of compound PMMB-317, 1 μM of colchicine and paclitaxel for 24 h,

respectively. After that, the dishes were washed with PBS for three times and fixed with 4% paraformaldehyde for 20 min, stained with 1% Triton-100 for 100 min. The cells were closed by 5% BSA under the condition of dark for 1 h. The liquid was removed and incubated with anti-tubulin antibody diluent (1:200, diluted by 3% BSA solution) over-night. The antibody was removed and washed with PBS for three times. 200 μL of Cy3-labeled goat anti-mouse IgG (H + L) (1: 1500 dilution) was added to each dishes and incubated for 1 h under dark condition followed by DAPI (1 μg mL^{-1}). The cells was observed by an Olympus confocal microscope and data was analyzed using FV-10-ASW 1.7 viewer.

3.4.9. In vitro microtubule assembly assay

An established method was performed to measure soluble (depolymerized) and assembled (polymerized) tubulin[29]. A549 cells (5×10^5 per flask) were seeded into the 75-T flask. Cells were exposed to colchicine (1 μM), paclitaxel (1 μM) and PMMB317 (8 μM) for 24 h. After treatment, cells were collected and washed twice with PBS then lysed at 37 ℃ for 5 min with 50 μL of hypotonic buffer. The cell lysates were centrifuged at 10000 rpm for 10 min at 25 °C. The supernatants containing soluble (cytosolic) tubulin were separated from the pellets containing polymerized (cytoskeletal) tubulin. The pellets were resuspended in 100 μL of hypotonic buffer, sonicated on ice, mixed with 5× sample buffer, and heated for 5 min at 100 °C. Equal amounts of the two fractions were partitioned by SDS-polyacrylamide gel electrophoresis. Immunoblots were probed with *β*-tubulin monoclonal antibody and secondary HRP-conjugated antibody. The blots were developed by using an ECL kit

and recorded by a digital camera (Tanon 5200, Tanon, China). Finally, the results were analyzed with Image J Software (National Institutes of Health, BetheSEMa, Maryland, USA).

3.4.10. Flow cytometry analysis of the expression of extracellular polymerized tubulin

A549 cells were plated in 6-well plates and treated with PMMB-317 (4, 8 μM), colchicine (1 μM), and paclitaxel (1 μM) for 24 h separately. After that, the dishes were washed with PBS for twice and blocked with 1% BSA for 30 min on ice, then were centrifuged (2000 rpm at 4 °C for 5 min) to remove supernatant. Then cells were incubated with *β*-tubulin antibody for 1 h on ice and were centrifuged (3000 rpm at 4 °C for 5 min) to remove supernatant. Next, cells were incubated with secondary antibody for 5 min) to remove supernatant. Finally, cells were then resuspended in PBS and the expression level of polymerized tubulin was analysed by flow cytometry (BD FACS Calibur, USA).

3.4.11. ROS generation analysis

Intracellular ROS were detected by using the total ROS detection kit (YEASEN, Shanghai, China) according to the manufacturer's instructions. Briefly, cells were seeded in a 6-well plate at approximately 75% confluence. After indicated treatment, cells were washed with PBS and were either stained directly with ROS detection solution at 37 °C for 20 min, washed in serum-free medium thrice then analyzed by using flow cytometry (BD FACS Calibur, USA).

3.4.12. Wound-healing assay

A549 cells were planted in a tissue culture 6-well plate at an initial density of 2×10^5

cells per cm^2 overnight. A micropipette tip was used to create a wound in the monolayer by scraping after cells seeding and incubation for 24 h. Identical cell-free space was observed by phase-contrast microscopy (NIKON, Japan) and digital images were taken by cells at 0, 24 and 48 h. Subsequently, the NIH Image J image analysis software was used to outline the wound areas and analysis quantifies the reduced cell-free space, n = 3.

3.4.13. Transplantation of A549 cells into nude mice

Cultured A549 cells were washed with and resuspended in ice-cold PBS. Portions of the suspension (6×10^6 cells in 0.1 mL) were injected into the right flanks of female nude mice. Two weeks after the injection, the mice bearing tumors (an average size of 90 mm^3) were distributed into 5 groups (n = 8 mice per group) according to tumor volumes. PMMB-317 (2 mg/kg, 4 mg/kg), Shikonin (2 mg/kg) and Afatinib (4 mg/kg) were dissolved in DMSO and administered once every two days for 16 times by intraperitoneal injection. Vehicle (DMSO)-treated group was included as control. Body weight and tumor volumes were measured and recorded every two days. Long diameter (L) and short diameter (S) of a tumor were measured with a vernier caliper and the tumor volume was calculated using the following formula: $L \times (S)^2/2$. Thirty-two days after injection, the mice were killed and tumors were separated. Tumor weight was measured and tumor sections were fixed in paraformaldehyde. The rest of the sections were frozen in liquid nitrogen and stored at -80 °C.

3.4.14. Western blot assay

The A549 cells on 6-well plates were rinsed twice with cold PBS and lysed in RIPA

lysis buffer containing a protease inhibitor mixture at 1:100 dilution on ice for 30 min. The insoluble components of cell lysates were removed by centrifugation (10000 rpm at 4 °C for 10 min), and protein concentrations were measured using a Pierce BCA protein assay kit. Proteins were separated by sodium dodecyl sulphate-polyacrylamide gel electrophoresis (SDS-PAGE) and transferred onto polyvinylidene difluoride (PVDF) membranes. Membranes were blocked using skim milk and then incubated with diluted antibody (1:1000 dilution) at 4 °C with gentle shaking overnight. After washing five times, membranes were incubated with secondary antibody (1:3000-1:5000 dilution) for 1 h at room temperature. Detection was performed by an enhanced chemiluminescent reagent (Thermo Fisher Scientific, USA) according to the manufacturer's instructions. Bands were then recorded by a digital camera (Tanon 5200, Tanon, China). Finally, the results were analyzed with Image J Software (National Institutes of Health, BetheSEMa, Maryland, USA), and all the targeted proteins were normalized to GAPDH or *β*-actin.

3.4.15. Docking simulation

Molecular docking of the compounds binding the three-dimensional X-ray structure of tubulin (PDB code: 1SA0) and EGFR (PDB code: 5HG8) were carried out using Discovery Studio (version 3.5) as implemented through the graphical user interface DS-CDOCKER protocol. The aforementioned compounds were constructed, minimized and prepared. The crystal structures of the protein complex were retrieved from the RCSB Protein Data Bank (http://www.rcsb.org/pdb/home/home.do). All bound waters and ligands were eliminated from the protein. The types of interactions

between the docked protein with ligand-based pharmacophore model were analysed after the end of molecular docking.

3.4.16. 3D-QSAR

3D-QSAR was a reliable way for better understanding systematic SAR profile on the synthesized compounds and to discover better tubulin inhibitors. 75% of the compounds were utilized as a training set for QSAR modeling and remaining 25% (PMMB-315, PMMB-318, PMMB-320, PMMB-323, PMMB-325) were selected as test subset for verifying the dependability of the QSAR model by the DS 3.5. The anti-proliferative activities of the compounds was applied to QSAR analysis. The reliability of QSAR model could be assessed by the cross-validated correlation coefficient. Scrambled test (Y scrambling) was performed to investigate the risk of chance correlations.

4. Conclusion

Both tubulin and EGFR are the important targets of antitumor drugs. According to our previous studies, shikonin and its derivatives are effective inhibitors of tubulin[30-32]. Some researchers also proved that shikonin is an effective inhibitor of EGFR[33]. In this study, a new series of shikonin derivatives were obtained by introducing the pharmacophore structure of benzoylacrylic acid into shikonin skeleton. The anti-proliferation activity assay suggested that, compound PMMB-317 showed the best inhibitory activity against A549 cells. Further study showed that PMMB-317 could significantly lead to tubulin de-polymerization and cell cycle arrest, induce the decrease of mitochondrial membrane potential, increase in ROS production. The EGFR inhibitory activities in *vitro* suggested the superior EGFR inhibitory of PMMB-317 which together ultimately lead to the cell apoptosis of A549 cells in a dose-dependent and time-dependent manner. Moreover, cell migration was inhibited to limit the potential of distal metastasis. Besides, western blot analysis of apoptosis-related proteins indicated that PMMB-317 promoted the expression of pro-apoptotic proteins, including cleaved Caspase-3, cleaved Caspase-9 and cleaved PARP. Molecular docking results have demonstrated that PMMB-317 simultaneously bound to EGFR protein (5HG8) and tubulin (1SA0) through a variety of bonding, thereby contributing to its anti-tumor effect. Furthermore, the results in vivo was also positive, since the nude mice tumor growth was delayed and the survival rate was prolonged in the usage of compound PMMB-317. Therefore, we speculated that PMMB-317 potentially served as an inhibitor based on tubulin and EGFR protein, it appears to be an attractive

candidate for further consideration in developing anticancer agents.

Abbreviations

MTT, (3-(4,5-dimethyl-2-thiazolyl)-2,5-diphenyl-2-H-tetrazolium bromide); NMR, nuclear magnetic resonance spectrum; TLC, thin layer chromatography; TMS, tetramethylsilane; DMSO, dimethyl sulfoxide; PBS, phosphate-buffered saline; DAPI, 4',6-diamidino-2-phenylindole; BSA, bovine serum albumin; SAR, structure-activity relationship; EGFR, epidermal growth factor receptor; MAPK, mitogen-activated protein kinase; MMP, mitochondrial membrane potential; PMSF, phenylmethanesulfonyl fluoride, ROS, reactive oxygen species. AKT, anti-apoptotic kinase.

Author contributions

YHY, HYL, XMW and JLQ: the conception and design of the study. WXS, HWH, MKY, ZLW: performed experiments. YSW, JYF, YTL, MYW and JXB acquisition of data, analysis and interpretation of data. HYL and WXS: wrote the main manuscript text, prepared figures and statistical analysis. GHL, JLQ and XMW: technical and material support. YHY: final approval of the version to be submitted. All authors read and approved the final manuscript.

Conflict of interest

The authors declare no conflict of interest.

Acknowledgements

This research was supported by the National Natural Science Foundation of China (NSFC) (21702100, 31771413, 31670298, 21907051), the Program for Changjiang Scholars and Innovative Research Team in University (IRT_14R27), and the Fundamental Research Funds for the Central Universities (020814380057, 020814380058).

References

[1] M. Krause, D. Zips, H.D. Thames, J. Kummermehr, M. Baumann, Preclinical evaluation of molecular-targeted anticancer agents for radiotherapy, Radiotherapy and oncology: journal of the European Society for Therapeutic Radiology and Oncology, 80 (2006) 112-122.

[2] A. Suhardja, H. Hoffman, Role of growth factors and their receptors in proliferation of microvascular endothelial cells, Microsc Res Techniq, 60 (2003) 70-75.

[3] M.A. Lemmon, J. Schlessinger, Cell signaling by receptor tyrosine kinases, Cell, 141 (2010) 1117-1134.

[4] N.A. Turner, S.G. Ball, A.J. Balmforth, The mechanism of angiotensin Ii-induced extracellular signal-regulated kinase-1/2 activation is independent of angiotensin AT(1A) receptor internalisation, Cell Signal, 13 (2001) 269-277.

[5] B. Biteau, H. Jasper, EGF signaling regulates the proliferation of intestinal stem cells in Drosophila, Development, 138 (2011) 1045-1055.

[6] H.Q. Jiang, M.O. Grenley, M.J. Bravo, R.Z. Blumhagen, B.A. Edgar, EGFR/Ras/MAPK Signaling Mediates Adult Midgut Epithelial Homeostasis and Regeneration in Drosophila, Cell Stem Cell, 8 (2011) 84-95.

[7] C. Yewale, D. Baradia, I. Vhora, S. Patil, A. Misra, Epidermal growth factor receptor targeting in cancer: a review of trends and strategies, Biomaterials, 34 (2013) 8690-8707.

[8] G.X. Xia, W.T. Chen, J. Zhang, J.A. Shao, Y. Zhang, W. Huang, L.D. Zhang, W.X. Qi, X. Sun, B.J. Li, Z.X. Xiang, C. Ma, J. Xu, H.L. Deng, Y.F. Li, P. Li, H. Miao, J.S.

Han, Y.J. Liu, J.K. Shen, Y.P. Yu, A Chemical Tuned Strategy to Develop Novel Irreversible EGFR-TK Inhibitors with Improved Safety and Pharmacokinetic Profiles, J Med Chem, 57 (2014) 9889-9900.

[9] G.J. Riely, Second-generation epidermal growth factor receptor tyrosine kinase inhibitors in non-small cell lung cancer, J Thorac Oncol, 3 (2008) S146-S149.

[10] X.F. Chen, Q. Zhu, Y.Q. Liu, P. Liu, Y.M. Yin, R.H. Guo, K.H. Lu, Y.H. Gu, L.K. Liu, J.H. Wang, Z.X. Wang, O.D. Roe, Y.Q. Shu, L.J. Zhu, Icotinib Is an Active Treatment of Non-Small-Cell Lung Cancer: A Retrospective Study, Plos One, 9 (2014) e95897-95903.

[11] G.D. Yang, Y.A. Yao, J.Y. Zhou, Q. Zhao, Effects of icotinib, a novel epidermal growth factor receptor tyrosine kinase inhibitor, in EGFR-mutated non-small cell lung cancer, Oncol Rep, 27 (2012) 2066-2072.

[12] R. Perez-Soler, The role of erlotinib (Tarceva, OSI 774) in the treatment of non-small cell lung cancer, Clin Cancer Res, 10 (2004) 4238s-4240s.

[13] Z.T. Liu, Z.H. Chen, J.Y. Wang, M.Q. Zhang, Z.W. Li, S.B. Wang, B. Dong, C. Zhang, J. Gao, L. Shen, Mouse avatar models of esophageal squamous cell carcinoma proved the potential for EGFR-TKI afatinib and uncovered Src family kinases involved in acquired resistance, J Hematol Oncol, 11 (2018) 109-121.

[14] S.L. Liu, Y.H. Tang, X.R. Yuan, D. Yuan, J.Y. Liu, B.Y. Li, Y.F. Li, Inhibition of Rb and mTOR signaling associates with synergistic anticancer effect of palbociclib and erlotinib in glioblastoma cells, Invest New Drug, 36 (2018) 961-969.

[15] K.-i. Onoue, T. Shintou, C.S. Zhang, I. Itoh, An Efficient Synthesis of β-Aroylacrylic Acid Ethyl Ester by the Friedel–Crafts Reaction in the Presence of Diethyl Sulfate, Chemistry Letters, 35 (2006) 22-23.

[16] U. Sankawa, Y. Ebizuka, T. Miyazaki, Y. Isomura, H. Otsuka, S. Shibata, M. Inomata, F. Fukuoka, Antitumor activity of shikonin and its derivatives, Chemical & Pharmaceutical Bulletin, 25 (1977) 2392-2395.

[17] Y. Kashiwada, M. Nishizawa, T. Yamagishi, T. Tanaka, G.-I. Nonaka, Anti-AIDS Agents, 18. Sodium and Potassium Salts of Caffeic Acid Tetramers from Arnebia euchroma as Anti-HIV Agents, J Nat Prod, 58 (1995) 392-400.

[18] U. Ozgen, P.J. Houghton, Y. Ogundipe, M. Coskun, Antioxidant and antimicrobial activities of Onosma argentatum and Rubia peregrina, Fitoterapia, 74 (2003) 682-685.

[19] H.Y. Lin, Z.K. Li, L.F. Bai, S.K. Baloch, F. Wang, H.Y. Qiu, X. Wang, J.L. Qi, R.W. Yang, X.M. Wang, Y.H. Yang, Synthesis of aryl dihydrothiazol acyl shikonin ester derivatives as anticancer agents through microtubule stabilization, Biochemical pharmacology, 96 (2015) 93-106.

[20] X.J. Zhu, Y. Shi, J. Peng, C.S. Guo, N.N. Shan, P. Qin, X.B. Ji, M. Hou, The effects of BAFF and BAFF-R-Fc fusion protein in immune thrombocytopenia, Blood, 114 (2009) 5362-5367.

[21] H.Y. Lin, W.X. Sun, C.S. Zheng, H.W. Han, X. Wang, Y.H. Zhang, H.Y. Qiu, C.Y. Tang, J.L. Qi, G.H. Lu, R.W. Yang, X.M. Wang, Y.H. Yang, Synthesis, characterization and biological evaluation of formononetin derivatives as novel EGFR

inhibitors via inhibiting growth, migration and inducing apoptosis in breast cancer cell line, Rsc Adv, 7 (2017) 48404-48419.

[22] A.P. Venook, Epidermal growth factor receptor-targeted treatment for advanced colorectal carcinoma, Cancer, 103 (2005) 2435-2446.

[23] H.Y. Qiu, F. Wang, X. Wang, W.X. Sun, J.L. Qi, Y.J. Pang, R.W. Yang, G.H. Lu, X.M. Wang, Y.H. Yang, Design, Synthesis, and Biological Evaluation of Chalcone-Containing Shikonin Derivatives as Inhibitors of Tubulin Polymerization, ChemMedChem, 12 (2017) 399-406.

[24] H.Y. Lin, W. Chen, J. Shi, W.Y. Kong, J.L. Qi, X.M. Wang, Y.H. Yang, Design, Synthesis and Biological Evaluation of Cinnamic Acyl Shikonin Derivatives, Chemical biology & drug design, 81 (2013) 275-283.

[25] C.C. Cheng, K.F. Chou, C.W. Wu, N.W. Su, C.L. Peng, Y.W. Su, J. Chang, A.S. Ho, H.C. Lin, C.G. Chen, B.L. Yang, Y.C. Chang, Y.W. Chiang, K.H. Lim, Y.F. Chang, EGFR-mediated interleukin enhancer-binding factor 3 contributes to formation and survival of cancer stem-like tumorspheres as a therapeutic target against EGFR-positive non-small cell lung cancer, Lung cancer, 116 (2018) 80-89.

[26] X. Lu, S. Liu, M. Han, X. Yang, K. Sun, H. Wang, H. Mu, Y. Du, A. Wang, L. Ni, C. Zhang, Afatinib-loaded immunoliposomes functionalized with cetuximab: A novel strategy targeting the epidermal growth factor receptor for treatment of non-small-cell lung cancer, International journal of pharmaceutics, 560 (2019) 126-135.

[27] M.M. Hamed, S.S. Darwish, J. Herrmann, A.H. Abadi, M. Engel, First Bispecific Inhibitors of the Epidermal Growth Factor Receptor Kinase and the NF-kappaB

Activity As Novel Anticancer Agents, Journal of medicinal chemistry, 60 (2017) 2853-2868.

[28] Y.G. Zheng, J. Su, C.Y. Gao, P. Jiang, L. An, Y.S. Xue, J. Gao, Y. Liu, Design, synthesis, and biological evaluation of novel 4-anilinoquinazoline derivatives bearing amino acid moiety as potential EGFR kinase inhibitors, European journal of medicinal chemistry, 130 (2017) 393-405.

[29] S.W. Wang, S.L. Pan, Y.C. Huang, J.H. Guh, P.C. Chiang, D.Y. Huang, S.C. Kuo, K.H. Lee, C.M. Teng, CHM-1, a novel synthetic quinolone with potent and selective antimitotic antitumor activity against human hepatocellular carcinoma in vitro and in vivo, Molecular cancer therapeutics, 7 (2008) 350-360.

[30] H.Y. Lin, H.W. Han, L.F. Bai, H.Y. Qiu, D.Z. Yin, J.L. Qi, X.M. Wang, H.W. Gu, Y.H. Yang, Design, synthesis and biological evaluation of shikonin thio-glycoside derivatives: new anti-tubulin agents, Rsc Adv, 4 (2014) 49796-49805.

[31] J. Guo, X.F. Chen, J. Liu, H.Y. Lin, H.W. Han, H.C. Liu, S.C. Huang, B.K. Shahla, A. Kulek, J.L. Qi, X.M. Wang, L.J. Ling, Y.H. Yang, Novel Shikonin Derivatives Targeting Tubulin as Anticancer Agents, Chemical biology & drug design, 84 (2014) 603-615.

[32] S.K. Baloch, L.J. Ling, H.Y. Qiu, L. Ma, H.Y. Lin, S.C. Huang, J.L. Qi, X.M. Wang, G.H. Lu, Y.H. Yang, Synthesis and biological evaluation of novel shikonin ester derivatives as potential anti-cancer agents, Rsc Adv, 4 (2014) 35588-35596.

[33] Q.L. Zhao, N. Kretschmer, R. Bauer, T. Efferth, Shikonin and its derivatives inhibit the epidermal growth factor receptor signaling and synergistically kill glioblastoma cells in combination with erlotinib, Int J Cancer, 137 (2015) 1446-1456.

Conflict of interest

The authors declare no conflict of interest.

Graphical Abstract

Design, synthesis and biological evaluation of benzoylacrylic acid shikonin ester derivatives as irreversible dual inhibitors of tubulin and EGFR

Wen-Xue Sun[1,2†], Hong-Wei Han[1,2†], Min-Kai Yang[1,2], Zhong-Ling Wen[1,2], Yin-Song Wang[1,2], Jiang-Yan Fu[1,2], Yun-Ting Lu[1,2], Ming-Yue Wang[1,2], Jia-Xin Bao[1,2], Gui-Hua Lu[1,2], Jin-Liang Qi[1,2]*, Xiao-Ming Wang[1,2]*, Hong-Yan Lin[1,2]*, Yong-Hua Yang[1,2]*

[1]*State Key Laboratory of Pharmaceutical Biotechnology, Institute of Plant Molecular Biology, School of Life Sciences, Nanjing University, Nanjing, 210023, PR China*

[2]*Co-Innovation Center for Sustainable Forestry in Southern China, MOE Key Laboratory of Forest Genetics and Biotechnology, Nanjing Forestry University, Nanjing, 210037, PR China*

Compound **PMMB-317**, which obtained based on the modification of the natural product shikonin, could co-target tubulin and EGFR, serving as a potential therapeutic anticancer agent.